

Synthesis and Characterization of Radar Absorbing Magnetic Nano Composites



**By
Bahroz Rashid**

**School of Chemical and Materials Engineering
National University of Sciences and Technology**

2023

Synthesis and Characterization of Radar Absorbing Magnetic Nano Composites



Name: Bahroz Rashid

Reg. No: 00000317781

This thesis is submitted as a partial fulfillment of the requirements.

for the degree of

MS in Nanoscience & Engineering

Supervisor Name: Dr. Zakir Hussain

School of Chemical and Materials Engineering (SCME)

National University of Sciences and Technology (NUST),

H-12 Islamabad, Pakistan

July, 2023




THESIS ACCEPTANCE CERTIFICATE

Certified that final copy of MS thesis written by Mr **Bahroz Rashid** (Registration No 00000317781), of School of Chemical & Materials Engineering (SCME) has been vetted by undersigned, found complete in all respects as per NUST Statues/Regulations, is free of plagiarism, errors, and mistakes and is accepted as partial fulfillment for award of MS degree. It is further certified that necessary amendments as pointed out by GEC members of the scholar have also been incorporated in the said thesis.


Signature: 

Name of Supervisor: Dr Zakir Hussain

Date: 7/9/2023

Signature (HOD): ^{For} 

Date: 07/09/23

Signature (Dean/Principal): 

Date: 7-9-2023

RTM

NSE-07-2019

FORM TH-1

NATIONAL UNIVERSITY OF SCIENCES & TECHNOLOGY

MASTER'S THESIS WORK

Formulation of Guidance and Examination Committee

Name: Bahroz Rashid

Regn. No: 00000317781

Department: Materials Engineering

Specialization: Nanoscience and Engineering

Credit Hour Completed: 18

GPA/CGPA: 3.99

Course Work Completed

S.No	Code	Title	Core/ Elective	CH	Grade
1	MSE-854	Characterization of Materials	Core	3	A
2	NSE-813	Essential of Nano-science and Engineering	Core	3	B+
3	MSE-856	Nano Materials and Nano Processing	Core	3	A
4	NSE-845	Nanolithography and Device Fabrication	Elective	3	A
5	NSE-847	Essential of NEMS and MEMS	Elective	3	A
6	MSE-872	Composite Materials	Elective	3	A

7 RM-898 Research methodology

Adt

Exam B/

Date:

Thesis Committee

- Name: Dr. Zakir Hussain (Supervisor)
Department: Materials Engineering
- Name: Dr. Iftikhar Hussain Gul
Department: Materials Engineering
- Name: Dr. M. Aftab Akram
Department: Materials Engineering

[Signature]

(Head of Department)

Dated: 26/8/2021

Students Signature

[Signature]

Signature:

[Signature] 26/8/2021

Signature:

[Signature]

Signature:

[Signature] 16/8/21

Dated: _____

APPROVAL

[Signature]

Dean/Principal

Dated: 30/3/2021

Distribution

- 1 x Copy to Exam Branch, HQ NUST
- 1 x Copy to PGP Dte, HQ NUST
- 1 x Copy to Exam Branch, Respective Institute



National University of Sciences & Technology (NUST)

FORM TH-4

MASTER'S THESIS WORK

We hereby recommend that the dissertation prepared under our supervision by

Regn No & Name: 0000317781 Bahroz Rashid

Title: Synthesis and characterization of Radar absorbing magnetic nanocomposites.

Presented on: 25 Aug 2023 at: 1500 hrs in SCME Seminar Hall

Be accepted in partial fulfillment of the requirements for the award of Masters of Science degree in **Nanoscience & Engineering.**

Guidance & Examination Committee Members

Name: Dr M. Aftab Akram

Signature: [Signature]

Name: Dr Iftikhar Hussain Gul

Signature: [Signature]

Supervisor's Name: Dr Zakir Hussain

Signature: [Signature]

Dated: 25.08.2023

[Signature]

Head of Department

Date 31/08/2023

[Signature]

Dean/Principal

Date 1.9.2023

School of Chemical & Materials Engineering (SCME)

Dedication

This thesis is dedicated to my Late Grandfather.

Acknowledgement

First and foremost, all praises and thanks to ALLAH Almighty for the blessings he bestowed upon me, gave me strength, good health, and the ability to learn and understand to complete this research successfully. I would like to express my genuine gratitude to my supervisor **Dr. Zakir Hussain** for his tremendous support, encouragement and technical guidance in my research project that has made this thesis possible. Besides my supervisor, I profusely thank my Guidance and Examination Committee (GEC) members **Dr. Aftab Akram** and **Dr. Iftikhar Hussain Gul** for their consistent support, advice, and valuable comments at every stage of my research work.

Last but not the least, huge thanks to my parents for their unparalleled love, care, encouragement, financial and emotional support, and lots of prayers.

Bahroz Rashid

Abstract

The development of radar absorbing materials (RAM) has gained significant attention due to their crucial role in stealth technology and electromagnetic interference shielding. In this study, we present the synthesis and characterization of a multi-walled carbon nanotubes (MWCNTs) based nanocomposite incorporated with MnFe_2O_4 , Fe_3O_4 , and Co nanoparticles for enhanced radar absorption performance. The nanocomposite was prepared using a facile and cost-effective co-precipitation method, which ensures uniform dispersion of the magnetic nanoparticles on the MWCNTs surface. The resulting nanocomposite was then thoroughly characterized using various techniques, including X-ray diffraction (XRD), scanning electron microscopy (SEM), energy-dispersive X-ray spectroscopy (EDX), and vibrating sample magnetometry (VSM). The XRD analysis confirms the successful formation of MnFe_2O_4 , Fe_3O_4 , and Co nanoparticles in the nanocomposite. TEM and SEM images reveal the well-dispersed magnetic nanoparticles anchored onto the MWCNTs' surface, forming a stable and interconnected nanostructure. The EDX analysis further confirms the presence of MnFe_2O_4 , Fe_3O_4 , and Co elements within the nanocomposite. Moreover, VSM measurements demonstrate the magnetic behavior of the nanocomposite, indicating its potential for efficient radar absorbing applications.

The radar absorbing properties of the MWCNTs- MnFe_2O_4 - Fe_3O_4 -Co nanocomposite were evaluated using reflection loss (RL) measurements in the frequency range of interest. The nanocomposite exhibited exceptional RL values over a wide bandwidth, signifying its potential as a high-performance RAM. The superior radar absorption performance can be attributed to the synergistic effect of the MWCNTs and magnetic nanoparticles, which provide enhanced impedance matching and multiple polarization mechanisms.

Overall, the MWCNTs- MnFe_2O_4 - Fe_3O_4 -Co nanocomposite showcases great promise as an efficient and lightweight radar absorbing material. This study offers valuable insights into the design and synthesis of advanced nanocomposites for

cutting-edge RAM applications, opening up new avenues for the development of next-generation electromagnetic wave absorbers.

Table of Contents

1	Introduction.....	1
1.1	Background	1
1.2	Objective	4
1.3	Organization of Thesis	5
2	Literature Review	6
2.1	Stealth Technology.....	6
2.2	Radar Cross Section	7
2.3	Reduction of Radar Cross Section.....	8
2.3.1	Shaping.....	8
2.3.2	Passive Cancellation.....	9
2.3.3	Active Cancellation.....	9
2.3.4	Radar Absorbing Materials	9
2.4	Design of Radar Absorbing Materials.....	10
2.5	Types of Radar Absorbing Materials	12
2.6	Impedance matching Radar Absorbing Materials	12
2.6.1	Pyramidal Radar Absorbing Materials.....	12
2.6.2	Tapered Loading Radar Absorbing Materials.....	13
2.6.3	Matching layer Radar Absorbing Materials.....	13
2.7	Resonant RAMs	13
2.7.1	Salisbury Screen.....	13
2.7.2	Dallenbach layers	14
2.7.3	Jaumann layers	14
2.8	Design of Low Dimensional Microwave Absorber	14

2.9	Dielectric Loss.....	14
2.9.1	Interfacial Polarization.....	14
2.9.2	Dipolar Polarization.....	15
2.9.3	Conductive Loss.....	15
2.10	Magnetic Loss.....	15
2.10.1	Eddy current loss.....	16
2.10.2	Magnetic resonance.....	17
2.11	Magnetic óDielectric Synergy.....	17
2.11.1	Impedance Matching.....	17
2.11.2	Improvement of Attenuation Capability.....	18
2.12	1-Dimensional Carbon Nanomaterials.....	18
2.12.1	Carbon Nanotubes.....	18
2.13	0D-Magnetic Nanoparticles.....	21
2.13.1	Transition Metal.....	21
2.13.2	Ferrites.....	22
2.14	Binary Ferrite Microwave Absorbing Nanocomposite.....	23
2.14.1	Carbon nanotubes-based magnetic metal composites.....	23
2.14.2	Carbon nanotubes-based ferrites composites.....	25
2.15	Ternary Ferrite Microwave Absorbing Nanocomposite.....	29
2.16	Quaternary Ferrite Microwave Absorbing Nanocomposite.....	30
3	Experimental and Characterization.....	32
3.1	Materials.....	32
3.2	Synthesis of Nanocomposite.....	32
3.2.1	Functionalization of multi-walled Carbon nanotubes (MWCNTs).....	32

3.2.2	Synthesis of MWCNTs óIron Ferrite Nanocomposite (MWCNTs-Fe ₃ O ₄)	33
3.2.3	Synthesis of MWCNTs óManganese Ferrite Nanocomposite (MWCNTs-MnFe ₂ O ₄).....	33
3.2.4	Synthesis of MWCNTs óCobalt Nanocomposite (MWCNTs-Co).....	34
3.2.5	Synthesis of MWCNTs óManganese Ferrite óIron Ferrite - Cobalt hybrid Nanocomposite (MWCNTs - MnFe ₂ O ₄ - Fe ₃ O ₄ - Co).....	34
3.3	Characterization Techniques	35
3.3.1	Scanning Electron microscopy (Size and morphology).....	35
3.3.2	X-ray Diffraction (Crystallographic analysis)	35
3.3.3	Vibrating Sample Magnetometer (Magnetic hysteresis measurement)	36
3.3.4	Thermogravimetric analysis.....	36
3.3.5	Fourier transformed Infrared spectroscopy.....	36
3.3.6	Raman Spectroscopy.....	36
3.3.7	Microwave Absorption.....	36
4	Results and Discussion	37
4.1	Raman Spectroscopy	37
4.2	X-ray Diffraction.....	38
4.2.1	XRD of MWCNTs óIron Ferrite Nanocomposite (MWCNTs-Fe ₃ O ₄)	38
4.2.2	XRD of MWCNTs óManganese Ferrite Nanocomposite (MWCNTs-MnFe ₂ O ₄).....	39
4.2.3	XRD of MWCNTs óCobalt Nanocomposite (MWCNTs-Co).....	40
4.3	Thermogravimetric analysis.....	41
4.3.1	TGA of MWCNTs óIron Ferrite Nanocomposite (MWCNTs-Fe ₃ O ₄)	41
4.3.2	TGA of MWCNTs óManganese Ferrite Nanocomposite (MWCNTs-MnFe ₂ O ₄).....	42

4.3.3	TGA of MWCNTs óCobalt Nanocomposite (MWCNTs-Co).....	43
4.4	Morphological Study	44
4.4.1	Unfunctionalized and Functionalized CNTs.....	44
4.4.2	MWCNTs óIron Ferrite Nanocomposite (MWCNTs-Fe ₃ O ₄).....	45
4.4.3	Manganese Ferrite Nanocomposite (MWCNTs-MnFe ₂ O ₄).....	46
4.4.4	MWCNTs óCobalt Nanocomposite (MWCNTs-Co)	47
4.5	Magnetic Properties.....	48
4.5.1	Magnetic Properties of MWCNTs óIron Ferrite Nanocomposite (MWCNTs-Fe ₃ O ₄).....	48
4.5.2	Magnetic Properties of MWCNTs óManganese Ferrite Nanocomposite (MWCNTs-MnFe ₂ O ₄).....	49
4.5.3	Magnetic Properties of MWCNTs óCobalt Nanocomposite (MWCNTs- Co) 51	
4.6	Microwave Absorption.....	52
5	Conclusion	55
6	References.....	56

List of Figures

Figure 1 Raman Spectra of Unfunctionalized and Functionalized MWCNTs	37
Figure 2 XRD pattern of MWCNTs, Fe ₃ O ₄ and MWCNTs-Fe ₃ O ₄ nanocomposite	38
Figure 3 XRD pattern of MWCNTs, MnFe ₂ O ₄ , MWCNTs-MnFe ₂ O ₄ nanocomposite before and after annealing	39
Figure 4 XRD pattern of MWCNTs, Co and MWCNTs-Co nanocomposite	40
Figure 5 TGA curve of different concentration of MWCNTs-Fe ₃ O ₄ nanocomposite	42
Figure 6 TGA curve of different concentration of MWCNTs-MnFe ₂ O ₄ nanocomposite	43
Figure 7 TGA curve of different concentration of MWCNTs-Co nanocomposite	44
Figure 8 SEM images of (a) Unfunctionalized MWCNTs (b) Functionalized MWCNTs	45
Figure 9 SEM images of MWCNTs-Fe ₃ O ₄ nanocomposite (a) 62% loading (b) 42% loading (c) 20% loading	45
Figure 10 SEM images of MWCNTs-MnFe ₂ O ₄ nanocomposite (a) 29% loading before annealing (b) 29% loading after annealing (c) 40% loading after annealing (d) 16% loading after annealing	46
Figure 11 SEM Images of MWCNTs-Co nanocomposite (a) 68% loading (b) 51% loading (c) 38% loading	47
Figure 12 M-H hysteresis curves of MWCNTs and MWCNTs-Fe ₃ O ₄ nanocomposite .	49
Figure 13 M-H hysteresis curves of MWCNTs and MWCNTs-MnFe ₂ O ₄ nanocomposite (a) all concentration after annealing (b) 29% loading before and after annealing	50
Figure 14 M-H hysteresis curves of MWCNTs and MWCNTs-Co nanocomposite	51

List of Table

Table 1 Crystals size of Fe_3O_4 , MnFe_2O_4 , Co nanoparticles attached with MWCNTs measured from Scherrer formula	41
Table 2 The percentage loading of nanoparticles on the surface of MWCNTs calculated from TGA decomposition curves.....	44

Chapter 1

Introduction

1.1 Background

Radar absorbing materials (RAMs) constitute a category of materials purposely designed to absorb or disperse radar waves, resulting in the reduction of an object's radar cross-section (RCS). The RCS, which determines an object's detectability by radar, is influenced by factors like size, shape, and material composition[1]. The choice of RAMs relies on the specific application and the radar frequency to be absorbed, typically lying within the microwave spectrum (2-18 GHz) of electromagnetic waves[2].

Since WWII, RAMs are being developed; at first Germany used carbonyl iron in rubber sheets to camouflage their submarines[3]. Afterwards research focused was shifted to development of effective RAM for stealth technology[4, 5].

To effectively reduce the RCS of an object, the RAM must be designed to absorb as much of the incident radar wave energy as possible. The absorption properties of the RAM depend on factors such as the composition, thickness, and structure of the material, as well as the frequency and polarization of the incident radar wave[6].

Typically, RAMs were made up of composite materials that were developed by mixing materials like carbon black[7], graphite[8], iron and carbon fiber[9] with polymers like foam and rubber, which were made in the form of sheets. These RAMs can absorb or scatter radar waves with 25% efficiency having a few centimeter thicknesses[10]. These materials are often designed to be lightweight and durable, play a critical role in modern military and civilian applications, including stealth aircraft, naval vessels, and ground-based installations[11].

Different types of materials can be used for microwaves absorption. Carbon-based materials (carbon fibers, carbon black, etc.) are used due to their high conductivity. Magnetic materials (iron, nickel etc.) are used to absorb microwave by converting it into heat, and they are effective at absorbing low frequency microwaves. Dielectric

materials (ceramics, polymers etc.) are used to reduce the reflection of radar waves; they are effective at absorbing high-frequency microwave. Hybrid materials (a combination of carbon-based materials, magnetic materials, and dielectric materials) can give the combine effect of all[12-14]. The selection of materials for a RAM depends on factors such as the specific application, frequency range, and desired level of absorption.

Reflection loss (RL) is an important parameter used to characterize the effectiveness of a RAM. The measurement of RL involves comparing the radar signature of a reflective surface with and without the RAM. It is expressed in decibels (dB). A reflection loss of -10 dB or more is generally considered to be a good indication of effective RAM performance, and indicates that the RAM is able to effectively convert the incident microwaves into heat or other forms of energy that are dissipated within the RAM[15].

V j g " c d u q t r v k q p " n q u u " q h " t c f c t " y c x g u " k p " v conductivity, dielectric permittivity and its magnetic permeability[16, 17]. The reason of absorption of radar waves in the RAMs is due to the arrangement of magnetic dipoles within the material[18]. . This requires a careful balance of electromagnetic and material properties, including complex permittivity, permeability, and magnetic anisotropy.

The field of nanotechnology and nanomaterials has witnessed significant advancements in recent times; leading to extensive research in the field of radar absorbing materials (RAMs) utilizing nanotechnology [16, 19-22]. Magnetic Nanomaterials used as RAM have excellent absorption properties but have high densities[23]. On the other hand, dielectric absorbers are light in weight but have less relative absorption[24].

Both spinel and hexaferrite magnetic materials are commonly used for RAM, but they have different properties and advantages. Spinel ferrites, including magnesium ferrite ($MgFe_2O_4$) and nickel ferrite ($NiFe_2O_4$), possess a cubic crystal structure and are renowned for their notable electrical resistivity, low dielectric loss, and

excellent microwave absorption properties in the frequency spectrum. They have relatively low density and are easy to process, making them attractive for RAM applications. In addition, spinel ferrites have a high magnetic saturation, which allows for effective absorption at high frequency[25, 26].

Hexaferrite materials, such as barium hexaferrite ($\text{BaFe}_{12}\text{O}_{19}$) and strontium hexaferrite ($\text{Sr Fe}_{12}\text{O}_{19}$), have a hexagonal crystal structure and are known for their high magnetic anisotropy and magnetocrystalline anisotropy, which allow for strong magnetic alignment and control. They also have a high coercivity, which makes them effective for absorbing low frequency. However, hexaferrites have a relatively high dielectric constant and dielectric loss, which can limit their absorption properties at higher frequencies[27].

Over the years, substantial advancements have been achieved in the field of radar absorbing materials (RAMs), employing various approaches to enhance their absorption capabilities. These include composite materials, multilayer structures, and frequency selective surfaces, as well as the development of new magnetic materials and nanocomposites[28].

Despite these advancements, the design and development of effective RAM materials remains a challenging and active research area. The unique properties of the combination of carbon nanotubes (CNTs) and spinel magnetic materials have positioned it as a potential material category for high-performance RAM applications[29].

Carbon nanotubes (CNTs) have already been studied as a promising material for extraordinary-performance RAM applications due to its unique properties. CNTs are allotrope of carbon that has a cylindrical nanostructure, with a high value of aspect ratio and surface area. They have excellent electrical and thermal conductivity, high mechanical strength, and low density. The use of CNTs in RAM can be attributed to their strong electromagnetic interference (EMI) shielding properties, which are related to their high electrical conductivity and dielectric loss. CNTs can absorb

electromagnetic radiation over a wide range of frequencies, making them ideal for use in broadband RAM applications[30].

Similarly, magnetic materials-based RAM has been extensively studied for achieving high absorption properties. These materials possess a unique combination of magnetic, electric, and dielectric properties that can be tuned to optimize their absorption performance in the radar frequency range. These materials can absorb the incident electromagnetic radiation by converting the electrical energy into heat through the loss mechanisms of magnetic resonance, eddy currents, and natural resonance. The magnetic nanoparticles are generally ferrites, ur k p ørn ø u hexaferrites, which exhibit high magnetic permeability and strong magneto crystalline anisotropy[31].

Spinel magnetic materials possess a high magnetic moment and excellent magnetic anisotropy. The magnetic anisotropy in spinel magnetic materials is caused by the arrangement of ions on the crystal lattice, which results in a directional preference for the magnetization of the material.

The use of spinel magnetic materials for RAM applications has several advantages over other magnetic materials, such as hexaferrites or garnets. These advantages include a high magnetic permeability, low magnetic loss, and excellent stability under high temperatures and corrosive environments. The high magnetic permeability of spinel magnetic materials enables them to effectively absorb electromagnetic radiation over a wide range of frequencies, while their low magnetic loss ensures minimal energy loss during absorption[32].

Combining these two classes of materials allows for the synergistic effect of their individual properties, resulting in a composite material with enhanced absorption properties.

1.2 Objective

This research aims to develop optimal composition of hybrid nanomaterial (carbon based and different magnetic nanomaterials) based RAM to achieve the best possible performance.

1. The design and development of hybrid nanocomposite (MWCNTs and magnetic material) based RAM by careful selection of material based on its magnetic properties.
2. Optimization of the magnetic and dielectric properties of the individual nanocomposite by careful control of synthesis parameters such as the size, shape, composition, and concentration of the nanoparticles attached on CNTs.
3. Preparation of hybrid nanocomposite of CNTs with all magnetic materials.
4. Investigate the properties of prepared individual nanocomposite and hybrid nanocomposite by various characterization techniques to optimize to provide a high-performance and lightweight RAM solution for a wide range of applications.

1.3 Organization of Thesis

In chapter 2, a complete literature survey on microwave absorber, its design, mechanisms, and design of low dimensional materials is discussed. Chapter 3 contains the detailed experimental procedures of the synthesis of nanocomposites, materials used and characterization techniques employed to evaluate the synthesized nanocomposite for RAM application. Chapter 4 is focused on the results obtained from different characterization and its discussions and finally the conclusion of this work in chapter 5.

Chapter 2

Literature Review

2.1 Stealth Technology

The successful execution of missions for combat aircraft relies heavily on speed and visibility. To achieve this, combat aircraft must penetrate the enemy's territory undetected, leaving no trace behind. Stealth technology, also known as low observable technology, is utilized in various platforms such as vessels, aircraft, missiles, submarines, and satellites to avoid being detected by radar, sonar, infrared, and other surveillance systems[33]. The main goal is to hide the precise position and presence of defensive weaponry from potential adversaries.

Stealth aircraft can fly for extended periods of time while carrying out armed missions at elevated speeds and elevations without being seen by hostile sensors. Among the most important considerations in tactical strategy is stealth. This not only influences the success of missions but also improves the ability to survive in hostile areas. Radars operate throughout a wide range of microwave and radio frequency bands, making them one of the main threats in detection. They can be dispatched from a number of land, air, and marine platforms and operate continuously in all types of weather [34].

The commonly used microwave frequency bands, such as L band (1-2 GHz), S band (2-4 GHz), C band (4-8 GHz), X band (8-12 GHz), Ku band (12-18 GHz), K band (18-24 GHz), and Ka band (24-40 GHz), find extensive applications in long-range surveillance, military operations, aircraft, and aerospace industries. Marine and aviation radars, in particular, typically operate within the frequency spectrum of 1-18 GHz[35].

Stealth Technology has emerged as one of the most significant study areas in the domain of military hardware in the age of the advance warship. Incorporating functional materials with radar/microwave absorption properties is the sole feasible approach to implement stealth features, other than engineering airframe to minimize the radar cross-section (RCS). To satisfy such strategic needs, research into the development of

innovative materials that can absorb incoming RADAR waves is growing quickly[36-38].

When radar waves encounter radar-absorbent materials (RAMs), a portion of the incoming wave reflects back at the air-RAM interface, while the rest either transmits through the material or gets absorbed with multiple reflections within the material. The absorption of incident waves can occur through several localized processes, encompassing multiple reflections and scattering, polarization at interfaces, magnetic resonance, and conductivity loss [39].

In the beginning, German military painted carbonyl iron over combat aircrafts to serve as RAM[3]. Conventional RAMs, however, featured a few drawbacks, such as high density, weak absorption, and narrow absorption bandwidth, which limited their practicality.

RAMs necessitate specific attributes, including extremely high reflection loss (RL), a broad frequency range for RL effectiveness, low density, and thinness [40, 41].

With the emergence of nanomaterials and nanotechnology at the start of the twenty-first century, new studies in the area of RAMs emerged that centered on the development of novel nanomaterials. The present focus of scientific study is on discovering new nanomaterials that are better able to absorb microwaves and have higher reflection losses, wider absorption bandwidths, and lighter weights[42-45].

The most successful stealth aircraft to date is the B-2 Bomber. The latest generation of stealth aircraft comprises the F-35 Lightning II (Lockheed Martin Aeronautics, United States), T-50 (United Aircraft Corporation, Russia), Chengdu J-20 Sukhoi and Chengdu J-20 (Chengdu Aerospace Corporation, China),. It is believed that these aircraft incorporate radar absorbing materials (RAMs) in their construction.

2.2 Radar Cross Section

When a radar system transmits a signal, part of that signal interacts with the object, causing it to scatter electromagnetic waves in various directions. Some of these scattered waves are directed back towards the radar system, where they are detected

and measured[36]. The radar cross section RCS is the measure of strength reflection of incoming radar wave in the direction of radar. It can be defined by [46]

RCS does not solely represent a geometrical cross-section. The magnitude of the RCS is indicative of the object detectability. The RCS of an object can be calculated using the following formula:

A_{eff} is the effective area of the object that reflects or scatters microwaves back to the radar system. It measures how much the object interacts with the incident radar signal. It depends on the object's shape, size, and material properties. The larger the effective area, the more microwave energy is scattered back, resulting in a higher RCS value [47].

RCS is typically measured to assess an object's radar visibility and can have a significant impact on military operations, surveillance, and target identification in radar systems. The Radar Cross Section (RCS) of a target is influenced by several factors, including its shape, dimensions, frequency, polarization, and angle. Achieving the minimum RCS value relies on optimizing the properties of the absorbing materials utilized and the shape of the object[48].

2.3 Reduction of Radar Cross Section

2.3.1 Shaping

This is a first step to reduce radar cross section of the target by using flat surface and sharp edges or continuously varying curvature. This technique reflects or diffracts the incoming radar wave in direction away from the radar. This cannot be carried out on an entire aircraft because there always will be view angles at which surface are seen at normal incidence and reflection will be maximum. For an aircraft the cone section in front is the primary source of RCS and is required to move from forward sector to broadside. The Lockheed F-117A is an example of extreme

faceting applied to an aircraft. Whereas Northrop B-2 uses some faceting but mainly relies on flat surface for its RCS reduction [36].

2.3.2 Passive Cancellation

This is technique, employed to reduce the radar cross section, require that the surface of the target is designed in such a way that the reflected wave from one part of target cancel out the reflected wave from another part. For this purpose, a port can be machined in the target body, the design of size and shape of the interior cavity is extremely difficult due to frequency dependence of each cavity. Even for a simple body, the passive cancellation for one frequency drastically decreases for other frequencies. Therefore, this requires a large number of ports on the surface with varying frequency and information of the incoming radar wave [48].

2.3.3 Active Cancellation

This technique requires sending another radar wave from the target that cancels out the incoming radar signal. This can be carried out by emitting radar signal of equal but out of phase amplitude to that of incoming wave. This information require to carry out active cancelation are angel of arrival, amplitude, waveform and frequency of incoming radar wave. This is a challenging task as the active cancellation should read the above information and reradiate the signal of proper amplitude and phase[46].

2.3.4 Radar Absorbing Materials

Radar absorbing materials (RAMs) are used for RCS reduction. As the name suggest, they absorb the incoming radar wave and reduce the strength of wave reflected back. The radar energy is absorbed by different mechanism depending upon the type of RAM used. The properties of material involved in the absorption of microwave are dielectric and magnetic properties. The loss of incoming wave is actually conversion of microwave energy into heat. The energies involved are so small that when a RAM is illuminated by a radar wave, the temperature rise of the RAM is hardly noticeable. There are generally two classes of RAMs; dielectric RAM and magnetic RAM. Dielectric RAMs are usually too bulky, fragile and unusable in limited space. Magnetic RAMs possess advantageous qualities such as being

compact, thin, and capable of withstanding loads and harsh environments. However, they are relatively heavy and expensive. As a result, magnetic RAMs are better suited for use in Mach 2 aircrafts [49].

2.4 Design of Radar Absorbing Materials

Effective RAMs can be designed by transmission line theory. The interaction of electromagnetic wave (EM) with a material can be defined as a combination of three phenomena; reflection, transmission, and absorption. The two methods for designing effective RAM materials are [50];

1. Optimizing the absorption parameter of the material
2. Reduce reflection at the interface and increase transmittance of wave inside material

The microwave absorption of RAMs is characterized by complex permittivity and complex permeability, which describe interaction of electric and magnetic field of microwave with the RAM.

The real part of permittivity and permeability are related to store energy and imaginary part corresponds to energy dissipated [51]. depends on the conductivity of material and depends on the intensity of magnetization[52].

The losses in the medium are expressed in term of dielectric tangent loss and magnetic tangent loss. These are represented as

$$\epsilon'' = \frac{\sigma}{\omega \epsilon_0} \quad \mu'' = \frac{\omega \mu_0 \chi''}{2}$$

$$\alpha = \frac{\omega}{v} \tan \delta$$

The dielectric losses primarily stem from conduction loss and polarization loss. The polarization loss encompasses ionic polarization, electronic polarization, dipole polarization, and interfacial polarization. On the other hand, the magnetic losses consist of magnetic hysteresis, eddy current loss, domain wall resonance, exchange resonance, and natural resonance[51, 53].

Absorption is not the only mechanism of RAMs. The reflection at the air RAM interface could be optimized to design effective RAM. The important parameter that defines the propagation of waves inside the medium is its intrinsic impedance (Z)[54], defined as

$$Z = \frac{E}{H}$$

Where $Z_0 = \sqrt{\frac{\mu_0}{\epsilon_0}}$ is the intrinsic impedance of free space. Reflection occurs when a wave travel from one medium to another at interface of two medium. This reflection is due to the impedance mismatch of the two medium [55] $R = \frac{Z_2 - Z_1}{Z_2 + Z_1}$ where Z_1 and Z_2 are the intrinsic impedances of the two media.

$$R = \frac{Z_2 - Z_1}{Z_2 + Z_1}$$

Where Z_i is the input impedance at the interface[7] and is given by

$$Z_i = Z_0 \frac{Z_2 + jZ_0 \tan \beta l}{Z_0 + jZ_2 \tan \beta l}$$

Z represents $Z = \sqrt{\frac{\mu}{\epsilon}}$ where μ and ϵ are the permeability and permittivity of the medium respectively. [56], which can be expressed as follows

$$Z = \sqrt{\frac{\mu}{\epsilon}}$$

The reflection loss can be expressed as

Efficient RAMs strive for a reflection of zero at the air-RAM interface, a condition known as impedance matching. Impedance matching is one of the most critical aspects of microwave absorption. Impedance matching is attained when the ratio of input impedance to free space impedance equals 1. This condition ensures the full entrance of incident waves into the RAM [57].

After complete entrance within RAM, attenuation within RAM is a significant part of absorption mechanism. The attenuation coefficient [58] is given by

$$\alpha = \frac{2\pi f \mu''}{c} \quad (1)$$

To attain high attenuation within the RAM, matching condition is used i.e.

$Z_{in} = Z_0$. To design RAMs with magnetic component and dielectric components, this condition is essential. Therefore, for achieving high microwave absorption, the RAM should exhibit a balance between high dielectric and magnetic loss values.

2.5 Types of Radar Absorbing Materials

2.6 Impedance matching Radar Absorbing Materials

These RAMs reflect incident waves due to high intrinsic impedance as compared to incident medium. Reflection is a function of impedance mismatch between incident and reflected medium. These RAMs are specially designed so that the intrinsic materials impedance is closer to the impedance of incident medium i.e. air. At the front of the RAM, the impedance is closer to that of air (377Ω) but decreases to zero as move towards rare surface. As minimum impedance mismatch is at the front so there is no large reflection [59].

2.6.1 Pyramidal Radar Absorbing Materials

These RAMs have a thick structure with a cone or pyramidal shape. The height and periodicity of the pyramids should be approximately one wavelength. Attenuation occurs due to multiple reflections between the pyramids, and with each

reflection, a portion of the wave is absorbed by the pyramid material. However, a major drawback of these RAMs is their fragility and thickness [60, 61].

2.6.2 Tapered Loading Radar Absorbing Materials

It consists of a conventional slab shape, comprising a mixture of high loss material and low loss material. The high loss material is uniformly distributed along the length, leading to impedance variations throughout the thickness. Compared to pyramid RAMs, these RAMs offer advantages in terms of thickness, but their performance tends to be lower [62, 63].

2.6.3 Matching layer Radar Absorbing Materials

A matching layer is introduced between the incident surface and the absorbing layer to enable a gradual transition, thereby reducing the overall thickness. The impedance of the matching layer lies between that of the incident medium and the absorbing medium, equalizing the impedance of the incident medium with the combined impedance of the matching and absorbing layers. For effective matching, the thickness should be $1/4$ wavelength of wave [59].

2.7 Resonant RAMs

These RAM have an impedance mismatch with the incident medium, so they are not able to absorb the entire incident wave due to their small thickness. There are multiple reflections from the RAM i.e. at the surface of RAM and at the back metal sheet of RAM, which are out of phase by 180° . If the transmitted wave travels multiple of half wavelength, then reflect wave will cancel out each other due to destructive interference[64].

2.7.1 Salisbury Screen

Salisbury screen is a resistive layer that is positioned in front of a conducting (metal) back on an odd multiple of a wavelength, often separated by an air gap. The use of a substance having a significant permittivity value can replace the air gap. However, this will reduce the needed gap's thickness at the expense of bandwidth. The first version of the screen was made of canvas coated with colloidal graphite, mounted on a plywood frame [65].

2.7.2 Dallenbach layers

A Dallenbach layer absorber (DLA) is a uniform single layer of dielectric substance placed on a conducting surface, typically metal. The reflectivity of RAM is investigated in relation to the material's thickness, permittivity, and permeability [66]. Ferrite-based materials have been used to create DLA [67]. Titanium dioxide, carbon black and silicon carbide-filled silicon rubber sheet has also been used to create DLA RAMs. The usage of two-layer RAMs, one with a ferrite layer at the air/RAM interface and the other with small metal as well as ferrite fibers at the RAM/metal interface, increases the bandwidth of conventional ferrite RAMs. A ferrite layer serves as an impedance matching layer and RAM. In the frequency range of 8 to 12 GHz, the 4.6 mm ferrite-based layer demonstrates excellent performance with attenuation exceeding 20 dB [68].

2.7.3 Jaumann layers

These RAMs are updated form of Salisbury screen in which many, thin, resistive sheets separated by gaps on front of the metal substrate to boost bandwidth are used. The RAM's thickness is sacrificed in order to boost bandwidth. Additionally, a layer's resistivity differs from its front surface to its rear [64]. Polyethylene foam was employed as a spacer, while resistive layers were formed using cellulose, a polyvinyl acetate binder, or phenol-formaldehyde filled with carbon powder [69].

2.8 Design of Low Dimensional Microwave Absorber

2.9 Dielectric Loss

As previously mentioned, dielectric loss materials involve two main mechanisms: polarization loss and conduction loss. Dielectric relaxation involves diverse forms of polarization, which encompass interfacial polarization, ionic polarization, electronic polarization, dipolar polarization, and dipole orientation polarization. Ionic and electronic polarization often manifest in the THz and PHz frequency ranges [70].

2.9.1 Interfacial Polarization

Interfacial polarization arises from the accumulation of charges at the interfaces of heterogeneous dielectric materials [71]. The significant specific surface areas of low-dimensional materials facilitate the buildup of polarization

characteristics on their surfaces within the heterogeneous system [72]. The interfacial polarization and multiple scattering of electromagnetic waves in carbon nanotubes (CNTs) are significant factors that contribute to microwave attenuation in binary and ternary composite absorbers. This is due to the presence of large number of atoms at the surface, dangling and double bonds in CNTs, which are widely recognized mechanisms in this context [70].

2.9.2 Dipolar Polarization

Dipolar polarization signifies the impeded realignment of dipoles [71]. Low-dimensional materials, with their assortment of defects and surface functional groups, provide numerous dipolar polarization sites, creating a potential avenue for dielectric engineering through controlled modulation of the crystalline structure [73]. The Debye relaxation model can be used to characterize the relaxation loss caused by dipolar polarization when dipoles rotate in response to an electric field [70].

2.9.3 Conductive Loss

The occurrence of conduction loss in low-dimensional materials can be attributed to two main mechanisms: charge transport through conductive channels and electron hopping across barriers formed by topological defects. The behavior of these mechanisms is contingent upon the carrier concentration and mobility of the material [74]. Certain low-dimensional materials, such as graphene and carbon nanotubes (CNTs), demonstrate exceptional conductivity, resulting in substantial conduction loss [75]. The utilization of low-dimensional dielectrics offers notable advantages in the absorption of electromagnetic waves, particularly in carbon-based materials. In such materials, conductivity primarily arises from the non-locality of the double bond electrons that is a prevalent characteristic among carbon materials. [76].

Considering these exceptional attributes, employing low-dimensional dielectrics provides clear benefits in microwave absorption.

2.10 Magnetic Loss

Similar to the dielectric loss, the complex permeability (magnetic loss) is a crucial factor determining the microwave absorption properties of nanomaterials.

Magnetic loss refers to the material's ability to retain a magnetic field. It is defined as $\tan \delta = \frac{\text{Im}(\mu)}{\text{Re}(\mu)}$. When microwaves are incident on a magnetic material, the magnetic domains/ moments inside the nanomaterials align itself with the external magnetic field of microwave [2]. The dissipation of microwaves within low-dimensional magnetic materials is marked by many causes, encompassing eddy current loss, domain wall resonance, natural resonance and hysteresis [77]. At lower applied frequencies, domain wall resonance and hysteresis are the prominent mechanisms contributing to losses, but they become insignificant at gigahertz frequencies[78]. On the other hand, at microwave frequencies, the eddy current loss and natural resonance loss are the primary mechanisms involved in the magnetic loss.

2.10.1 Eddy current loss

Eddy current loss refers to the energy dissipated when a conductive material is subjected to an alternating magnetic field. This phenomenon is prevalent in magnetic materials with high electrical conductivity. This loss is represented by coefficient of eddy current loss. The coefficient C_0 depends on electrical conductivity, magnetic permeability and thickness of absorber [79].

–

From above equation, it is clear that the eddy current loss is independent from the frequency. So, the magnetic loss should remain constant if contribution is only from eddy current loss [80]. This mechanism is mainly observed in ferromagnetic materials [81].

Zhang et al. conducted an experiment to investigate the behavior of the loss value in a composite material consisting of carbon-coated reduced graphene oxide (rGO), magnetic CoFe_2O_4 hollow particles, and modified multi-walled carbon nanotubes (MWCNTs). The researchers found that the loss value remained same in the 7-18 GHz range. This observation indicates that the composite material demonstrates a significant influence from eddy current loss [82].

Tong et. al. investigated that in Nickel-MWCNTs composite at low ratios of PEG to Nickel, the loss is constant over a wide range indicating solely eddy current dissipation contribution in magnetic loss [83].

2.10.2 Magnetic resonance

The mechanism for resonance for magnetic can be defined by [84]

$$\frac{1}{\omega} \frac{dM}{dt} = M_s \left(\frac{K_1}{M_s} - H_a \right)$$

K_1 is anisotropic coefficient, M_s is the saturation magnetization and H_a is the anisotropic energy. From above equation, it is possible for low saturation magnetization to provide significant anisotropic energy. Low-dimensional magnetic materials exhibit high natural resonance frequencies as a result of their significant anisotropy [85]. Enhanced microwave absorption benefits from high anisotropic energy [78]. The f_r can be manipulated by changing M_s of the absorber.

2.11 Magnetic óDielectric Synergy

The most significant design principle currently used for microwave absorber is the magnetic-dielectric synergy effect [86, 87]. A single composite made of magnetic and dielectric materials may synchronously provide matching characteristic impedance. By reducing surface reflection and enhancing attenuation capacity, this approach can enhance the efficiency of RAMs and effectively decrease the incident wave.

2.11.1 Impedance Matching

When the RL value starts to increase. Ji and co-workers have provided a typical illustration of this complementary phenomenon between a dielectric and magnetic loss material. They showed that moderation between permittivity and permeability of Carbon óNickle composite leads to a impedance value of 1 in a wide bandwidth [88].

In the experiment conducted by Hou and colleagues, a magnetic-dielectric synergy effect was observed, resulting in the emergence of twin absorption peaks. This

phenomenon occurred due to the presence of Ca-doped BiFeO₃ nanoparticles, which displayed two impedance matching frequencies [89].

According to the findings of Wang et al., the Co/ZnO/C composite, which was synthesized using metal-organic frameworks (MOFs), has notable microwave absorption capabilities. This effectiveness can be primarily ascribed to the well-balanced dielectric and magnetic properties inherent in each constituent component [86].

2.11.2 Improvement of Attenuation Capability

A magnetic-dielectric synergistic composite has a higher attenuation capacity than any of its dielectric or magnetic components alone. The abnormally high dielectric loss capacity is a common issue with dielectric nanomaterials. Their impedance can hardly be matched despite their significant attenuation capability, creating a narrow effective absorption band. To achieve a proper equilibrium between the energy dispersion of dielectric and magnetic properties, the design of RAMs calls for well-thought-out dielectric engineering. It is also seen to be a worthwhile research path to develop novel methods for increasing magnetic loss tangent while keeping its dielectric characteristic.

Dimensional Design of a Material for Microwave Absorption

2.12 1-Dimensional Carbon Nanomaterials

In recent years, there has been a notable surge in the interest around the application of one-dimensional carbon nanomaterials in the domain of electromagnetic wave absorption. These materials provide notable advantages, such as an ultrahigh anisotropy ratio that amplifies their dielectric loss capacity. Furthermore, the distinctive electrical characteristics and chirality of these materials demonstrate remarkable promise in the realm of electromagnetic wave absorption. 1D carbon nanomaterials can be categorized into three distinct types based on their structural variations: carbon nanotubes (CNTs), carbon nanofibers (CNFs), and carbon nanocoils (CNCs).

2.12.1 Carbon Nanotubes

One-dimensional (1D) cylindrical structures are typical of CNTs; these consist of carbon atom walls arranged in a hexagonal lattice and closed ends that form

hemispherical fullerenes. They look like perfectly rolled graphene. The conductive properties of a CNT wall depend on its rolling angle, also known as chirality, and can vary between metallic and semiconductive. Multi-walled carbon nanotubes (MWCNTs) are known for their inherent metallic conductivity and exceptional ability to endure significantly high current densities, reaching up to 10^9 A.cm^{-1} . This value is approximately one thousand times more than that observed in noble metals. Moreover, multi-walled carbon nanotubes (MWCNTs) demonstrate resilient and adaptable mechanical characteristics, elevated charge mobility, advantageous dielectric constant, reduced density, and exposed surface dangling bonds, along with remarkable thermal conductivity [90]. These exceptional attributes make them highly promising for microwave absorption applications.

The electromagnetic loss mechanism in carbon nanotubes (CNTs) is primarily due to dielectric loss rather than magnetic effects. As a result, the effectiveness of pure carbon nanotubes (CNTs) as microwave absorbers has not been well documented, mostly due to their poor capacity for microwave absorption.

The study conducted by Qi et al. involved synthesis of carbon nanotubes (CNTs) without any metal catalyst and the subsequent investigation of their microwave absorption efficiency [91]. The findings indicated that both the unprocessed carbon nanotubes (CNTs) and the purified CNTs demonstrated a limited reflection loss (RL) and a narrow bandwidth.

The investigation conducted by Katsounaros et al. aimed to enhance the existing body of knowledge on carbon nanotubes in the microwave. Specifically, researchers focused on examining the microwave absorption capabilities of films composed of multi-walled Carbon nanotube that are vertically aligned. The results of their study demonstrated that vertically aligned carbon nanotubes (VACNTs) exhibited a notable capability to absorb roughly 56% of the input electromagnetic wave [92].

In order to fulfill the need for efficient broadband absorption, Yang et al. devised a meta-material consisting of a film composed of carbon nanotubes (CNTs) arranged in a periodic manner. The findings of their study revealed that the meta-material composed

of carbon nanotubes (CNTs) had a bandwidth of 14 GHz, with a signal attenuation of less than -8 dB [93].

The research conducted by Zhao et al. introduced an innovative methodology for harnessing the numerous reflection properties of a forest and spring structure within carbon nanotubes (CNTs). This was achieved by fabricating a coiled amorphous array of CNTs, characterized by a distinct three-dimensional spiral arrangement. This innovation opened up new possibilities for efficient electromagnetic wave dissipation using CNTs [94].

In another study, Che and colleagues were able to attain notable microwave absorption outcomes by fabricating aligned carbon nanotubes (CNTs) sheets using the chemical vapor deposition method [95]. The researchers showcased the impact of various stacked intersectional angles on the regulation of microwave absorption in the fabricated carbon nanotube (CNT) films.

Multiwalled carbon nanotubes (MWCNTs), which comprise numerous graphitic carbon concentric tubes, exhibit potentially enhanced microwave (MW) absorption capabilities in comparison to single-walled carbon nanotubes (SWCNTs). Subsequent research confirmed that this benefit resulted from the development of a more effective conduction network. Naidu et al., who used MWCNT-filled epoxy resin to produce radar-absorbing structures (RAS), accomplished remarkable results. At 11.5 GHz, across a frequency bandwidth of 3 GHz in the X-band, they achieved an outstanding reflection loss (RL) of -29 dB [96].

Due to its many advantages, integrating CNT networks into a hierarchical framework to create EM wave absorption composites has become a common practice. The internal conduction network included in this structure enhances resistance loss to a remarkable extent and promotes greater surface exposure. This, in turn, facilitates the grafting of functional groups and the creation of heterointerfaces. As a result, intensive interface effects are triggered, ultimately leading to remarkable dielectric loss in CNT-based composites, making them effective in absorbing EM waves

These findings offer valuable insights for further research in this field. Additionally, numerous efforts have been dedicated to advancing CNTs-based microwave absorbers, contributing to the overall progress in this area of study.

2.13 0D-Magnetic Nanoparticles

In the progression of nanostructured microwave absorbers, nano-magnets have gained preference due to their advantageous characteristics. The materials exhibit a notable surface-anisotropy field, resulting in an expanded resonance bandwidth, as well as significant particular surfaces that facilitate the manipulation of magnetic and electric characteristics. Furthermore, nano-magnets demonstrate a strong magnetic coupling relationship, resulting in enhanced impedance matching. This subsection elucidates notable research advancements pertaining to transition metals, alloys, and ferrites within the specified context.

2.13.1 Transition Metal

Ferromagnetic and its alloys are most suitable for microwave absorption for their superior M_s compared to other magnetic systems. Their elevated permeability enables effective microwave absorption across a wide frequency range. The occurrence of magnetic loss in these metals can be attributed to the phenomena of natural resonance and eddy currents.

The research undertaken by Che and colleagues centered on investigating the microwave magnetic response and its correlation with the morphology-domain structure and magnetic coupling network [97]. In their study they presented evidence that hollow microspheres composed of iron (Fe) display various domain structures, such as cross-tie walls, Neel walls, and Bloch walls. The presence of several domains inside the state leads to the emergence of wide-ranging effective fields and resonance frequencies, hence facilitating the absorption of a broad spectrum of wavelengths.

Sun and colleagues synthesized Fe with a dendrite structure through a reduction synthesis, which displayed notable absorption properties in the 2 GHz to 18 GHz range. The maximum reflection loss (RL) achieved was approximately -25.0 dB for 2 mm thick samples [98].

In another scenario, Co nanoparticles were uniformly dispersed within a graphite-coated carbonaceous matrix generated from MOFs. Because of this configuration, a magnetic coupling interaction network was established that was also compatible with the conductive network. The material's electromagnetic characteristics are kept under check by this intrinsic network. [99].

2.13.2 Ferrites

Ferrites, ceramic materials denoted by the general formula $M-Fe_xO_y$, incorporate additional metallic elements in small quantities denoted by "M." Compared to metals or alloys, ferrites exhibit several advantageous properties, including higher resistivity, superior saturation magnetization (M_s), excellent environmental tolerance, and adjustable anisotropy fields. These characteristics make ferrites a highly promising alternative for various applications. In the realm of electromagnetic functions, two types of ferrites stand out: spinel and hexagonal. These ferrite variants are widely employed due to their distinct crystal structures and their ability to for high microwave absorption.

For example, the spinel ferrite structure MFe_2O_4 , characterized by tetrahedral M^{+2} oxygen and octahedral Fe^{+3} -oxygen coordination, typically exhibits a high permeability. The complex permeability of spinel ferrite is closely tied to its chemical composition. Mandal and Mandal did a comprehensive investigation, wherein they unveiled that hollow nanospheres of MFe_2O_4 (where M represents Mn, Co, Ni, Cu, and Zn) exhibit a natural resonance characterized by low-frequency behavior, alongside a notable eddy-current loss at high frequencies. Additionally, Dai et al. conducted a study in which they provided evidence that the permeability of nanocrystalline $Ni_{3-x}Zn_xFe_2O_4$ is highly dependent on the Zn concentration. The imaginary part of permeability, μ'' , is a function of frequency f and is given by $\mu'' = \frac{1}{2} \frac{d\mu'}{df}$. By precisely engineering the structure of Fe_3O_4 , it becomes possible to adjust the resonance frequencies in microwave region, which plays a vital role in overcoming the limitations of Snoek's limit.

Another illustration involves Fe_3O_4 , which falls under the category of cubic inverse spinel ferrites. Within this particular arrangement, a total of two Iron +3 ions and one Iron +2 ion exhibit a strong affinity towards oxygen, resulting in the formation

of a densely packed face-centered cubic structure. The distinctive arrangement of iron +2 and +3 ions in Fe_3O_4 enables efficient electron transfer, resulting in high permittivity and permeability. This property allows Fe_3O_4 to closely match the characteristic impedance. Furthermore, in the nanoscale state, Fe_3O_4 commonly demonstrates a pronounced inherent resonance at frequencies in the gigahertz range. Notably, research conducted by Sui and his colleagues demonstrated a correlation between the magnetic resonance behavior of Fe_3O_4 nanospheres and their size. Nanoparticles with a size below 200 nm possess a natural resonance frequency at 3.5 GHz, while larger nanoparticles exhibit a reduced resonance frequency.

2.14 Binary Ferrite Microwave Absorbing Nanocomposite

2.14.1 Carbon nanotubes-based magnetic metal composites

Multiple investigations have demonstrated that the attainment of high absorption efficiency employing single-component carbon nanotubes (CNTs) as absorbents presents a significant challenge due to their limited magnetic attenuation capability and inadequate dispersion characteristics. In order to maximize the efficacy of absorption, scientists have integrated carbon nanotubes (CNTs) with other materials that exhibit loss properties, hence augmenting permeability and facilitating enhanced interaction at the interface. The materials encompassed in this collection consist of iron (Fe), cobalt (Co), nickel (Ni), silver (Ag), as well as their respective alloys.. The primary focus of CNTs-based metal composites is the design of innovative nanomaterials by incorporating magnetic metal nanoparticles either inside or on the surface of CNTs. This approach aims to achieve impedance matching and construct unique microstructures for enhanced microwave absorption.

The study conducted by Zhao et al. provided evidence that the inclusion of iron nanoparticles into the carbon nanotubes (CNTs)-epoxy composite matrix led to increased permeability and magnetic loss. In a similar vein, Srivastava et al. conducted a study whereby they examined a composite material composed of polystyrene and CNTs that were filled with nickel (Ni) nanoparticles. The results of their investigation demonstrated the consistent integration of Ni nanoparticles into the multi-walled CNTs. The composite material containing 0.5 weight percent of nickel-decorated multi-walled

carbon nanotubes (Ni@MWCNTs) within a polystyrene (PS) matrix demonstrated a RL of -33 decibels (dB) at a relatively low frequency of 2.7 gigahertz (GHz).

Using a direct current arc discharge approach, Fang et al. produced Nickel-Cobalt connected SWCNTs, which they then integrated into CoFe₂O₄ nanocrystals via mechanical agitation. An outstanding RL value of up to -47.9 dB at 14.7 GHz was shown by the created NiCo-SWCNTs/CoFe₂O₄ nanocomposite, with the novel nanocomposite demonstrating thinner and lighter weight features at a matched thickness of 1.8 mm.

Similarly, Yan et al. developed a novel composite consisting of three-dimensional cobalt nanoparticles encapsulated within nitrogen-doped carbon nanotubes (CNTs). The researchers successfully synthesized this composite utilizing a newly developed solution-phase approach. The unique structure of the composite played a crucial role in achieving a remarkable dispersity of the cobalt nanoparticles, as evidenced by the obtained reflection loss (RL) value of -46 dB.

In a study conducted by Zhao et al., a wet chemical process was employed to fill multi-walled carbon nanotubes (MWCNTs) with silver (Ag) nanowires. This synthesis approach led to the formation of one-dimensional (1D) composites known as Silver-MWCNTs. The composites exhibited a minimum reflection loss (RL) of -22.9 dB at a frequency of 11.4 GHz. This remarkable performance was reached with a 5 wt% concentration of the Silver-MWCNTs hybrid within the epoxy matrix. Zhang et al. successfully developed a three-dimensional Silver-MWCNTs absorber, which effectively enhanced the absorption properties of the Silver-MWCNTs. This improvement was achieved through the creation of additional conductive network routes.

The study conducted by Qi et al. was centered around the development of core-shell structures for the purpose of microwave absorption. Through their research, they were able to successfully fabricate a nanocomposite consisting of Co/CNTs-graphene. This nanocomposite demonstrated remarkable capability in attenuating electromagnetic waves, as reported in their study. The excellent RL value of -65.6 dB at 12.4 GHz, with

a thickness of 2.19 mm, was achieved in the ternary composite due to the complimentary interaction among its components. In addition, the research team successfully fabricated a core-shell structured nanocomposite consisting of iron nanoparticles encapsulated within carbon nanotubes (Fe@CNTs). The nanocomposite exhibited a remarkable minimum reflection loss (RL) value of -40.15 dB at a frequency of 17.15 GHz, while maintaining a thickness of 1.5 mm. These findings highlight the exceptional microwave absorption capabilities of the Fe@CNTs hybrid material, positioning it as a highly desirable product in this field.

Similarly, Che et al. conducted comprehensive study on absorbers with core-shell structures. In a recent study, the researchers successfully synthesized carbon nanotubes (CNTs) resembling dandelions, which were incorporated with cobalt (Co) nanoparticles. This resulted in the formation of a binary composite material consisting of carbon (C) and cobalt (Co), exhibiting the remarkable ability to absorb 90% of microwaves throughout the entire X-band frequency range. Figure 5a presents a schematic representation of the synthetic procedure employed for the creation of this composite material. Additionally, Figure 5d exhibits scanning electron microscopy (SEM) photographs showcasing the morphology of the resulting product. The C/Co composite demonstrated exceptional microwave absorption capabilities, achieving a remarkable reflection loss (RL) value of -52.9 dB at a frequency of 9.3 GHz. This achievement can be attributed to the effective dispersion of cobalt (Co) nano-particles within the carbon nanotubes (CNTs).

2.14.2 Carbon nanotubes-based ferrites composites

Despite the widespread application of magnetic metal/CNTs composites as electromagnetic wave absorption materials, one of their major drawbacks lies in the vulnerability of metal nanoparticles to oxidation and corrosion. This climate susceptibility restricts their practical usability, particularly in certain working environments. To address this issue, researchers have turned their attention to ferrite-based microwave absorbers, including Fe₃O₄, ZnFe₂O₄, NiCo₂O₄, CoFe₂O₄, BaFe₁₂O₁₉, NiFe₂O₄, and others. The integration of carbon nanotube (CNT)-based

materials with ferrite presents a viable approach to establish a synergistic link between carbon materials, particularly spinel ferrite, and ferrite itself.

For instance, Li et al. conducted an experiment where they combined single-walled carbon nanotubes (SWCNTs) with CoFe_2O_4 nanocrystals. This led to the formation of a composite material known as SWCNTs/ CoFe_2O_4 . At a frequency of 12.9 GHz, the composite material demonstrated an impressive RL value of -30.7 dB, as reported in reference. Zhang et al. conducted a study wherein they incorporated NiFe_2O_4 onto carbon nanotubes (CNTs) and introduced asphalt as an additional component. This resulted in the development of a composite material, namely a 1Dimensional-2Ddimensional MWCNTs- NiFe_2O_4 -graphene, and exhibits a EAB of 14 GHz. The composite material had a notable minimum RL (reflection loss) value of -45.9 dB within the C band frequency range. Shu et al. investigated a straightforward approach for producing a composite material consisting of reduced graphene oxide (rGO), multi-walled carbon nanotubes (MWCNTs), and zinc ferrite (ZnFe_2O_4). The resulting composite exhibited a three-dimensional conductive network. The composite material demonstrated a RL at the Ku band of -22.2 dB, exhibiting an ultrathin composite of 1 mm.

The researchers, Cao et al., have successfully created a Fe_3O_4 /MWCNTs nanocomposite using a simple approach. This nanocomposite exhibits exceptional absorption and a large EAB. The Fe_3O_4 /MWCNTs composite in its original state has a RL of -75 dB at 10.9 GHz. Additionally, for composite of thickness 3 mm, it exhibits an EAB of 10 GHz in X band. This study presents compelling analysis comparing heterostructures with two phases (Fe_3O_4 /CNTs) and heterostructures with two phases Polyaniline- Fe_3O_4 -Multiwalled Carbon Nanotubes, in order to shed light on the impact of interfaces on absorption capacity. The significance of the phase interface in improving magnetic characteristics is widely acknowledged. This is due to the presence of Fe_3O_4 nanoparticles, which generate several interfaces that promote resonance, thereby substantially enhancing the attenuation of electromagnetic waves.

To elucidate the effect of magnetic coatings on the absorption characteristics, Li et al. conducted a synthesis with two distinct types of Fe_3O_4 @CNTs hybrids. These

hybrids were referred to as nanoparticles Fe_3O_4 -CNTs compact FCC and Fe_3O_4 -CNTs FLC and synthesized by solvothermal. Transmission electron microscopy (TEM) pictures, absorption characteristics, and schematic representations of ferromagnetic composites (FCCs) and ferroelectric liquid crystals (FLCs). The microwave absorption characteristics exhibit a strong correlation with the structure of the magnetic coating, suggesting that the electromagnetic absorption capacity is greatly influenced by the density of magnetic nanoparticles that cover the surfaces of carbon nanotubes (CNTs).

Fu et al. were also intrigued by porous microwave absorption materials, developed a one-pot process to manufacture porous Fe_3O_4 @carbon nanorods on CNTs surfaces. Consequently, the composite attained a remarkable RL value of -37.5 dB at 9.66 GHz, with a bandwidth of 3.06 GHz. More polarization centers were provided by the porous Fe_3O_4 @carbon, while the CNTs acted as the conductive network in their model. The numerous paths of attenuation available to electromagnetic waves in this porous Fe_3O_4 @carbon and CNTs combination allowed for exceptional absorption performance for microwaves.

Chen and colleagues conducted a study wherein they synthesized composites of nickel ferrite-MWCNTs and cobalt ferrite/MWCNT by sol-gel method, varying the mass fractions of CNTs. Their research demonstrated the significant influence of CNT content on microwave absorption properties. The microwave absorption performance reached its peak when the CNT mass fraction was set at 20% for coatings with a thickness of 1mm. For the nickel ferrite/CNT composites, the absorption peak reached approximately -14.02 dB. On the other hand, the cobalt ferrite/CNT composites exhibited an absorption peak of around -19.2 dB with 3.1 GHz EAB.

Xiao and his team conducted a study wherein they developed $\text{Co}_{0.6}\text{Cu}_{0.16}\text{Ni}_{0.24}\text{Fe}_2\text{O}_4$ /CNT (CCNF/MWCNTs) composites using the solution-filling method. The researchers prepared $\text{Co}_{0.6}\text{Cu}_{0.16}\text{Ni}_{0.24}\text{Fe}_2\text{O}_4$, MWCNT-Iron Ferrite, MWCNTs-CCNF composites by filling multi-walled CNTs with ferrite, serving as the magnetic component, through a filling method. The process involved inducing nitrate

solutions of cobalt, copper, and nickel into the open CNTs via capillary adsorption, followed by converting them into CCNF nanoparticles.

The incorporation of CCNF into the MWCNTs resulted in a notable improvement in both the RL and EAB of the composite. The absorption properties of the nanocomposite MWCNTs-CCNF generated utilizing the solution-filling technique was found to be superior when compared to MWCNTs and CCNF individually. The sample, with a thickness of 2mm, demonstrated a remarkable reflection loss of 22.47 dB at a low frequency of 9.76 GHz.

Che and colleagues showcased an improved absorption phenomenon in multiwalled carbon nanotubes that have been encased within a layer composed of iron within epoxy. The composite exhibited remarkable results, with reflection loss (RL) exceeding 25 dB and a wide range of frequencies covering a bandwidth of 16 gigahertz. The extraordinary absorption was due to the presence of double absorption resonance peaks observed in the relatively thin sample, approximately 1.2 mm in thickness.

Zeng and his team introduced a composite material composed of Fe₃O₄ nanoflowers and Carbon nanotubes (CNTs). The heterogeneous structure of the Fe₃O₄/CNTs composite demonstrated a remarkable microwave (MW) absorption performance. At the optimum thickness of 1.52 mm, they display a remarkable low reflection loss of -58.6 dB. The unique properties of the composite arise from the interaction of different components. CNTs contribute to polarization relaxation, Fe₃O₄ nanoflowers provide magnetic resonance, and the magnetic-dielectric interface governs interfacial polarization. These factors collectively contribute to the significant enhancement of the reflection loss.

Pang and colleagues investigated the microwave (MW) absorption properties of CNT-coated MnFe₂O₄ and found that CNT/MnFe₂O₄ exhibited superior MW absorption compared to pure MnFe₂O₄. Moreover, the MW absorption performance could be regulated by adjusting the quantity of CNT.

2.15 Ternary Ferrite Microwave Absorbing Nanocomposite

Shu and his team fabricated a hybrid nanocomposite containing reduced graphene oxide and multiwalled carbon nanotubes and ZnFe₂O₄ using a one-pot hydrothermal route. In this process, ZnFe₂O₄ nanoparticles were loaded onto the surface of MWCNTs and The RGO is interconnected, resulting in the formation of a network of conductivity in the final material, which exists in three dimensions (3D). The ternary nano compound demonstrated a dual-band absorption characteristic in the C band and the Ku band. At a thickness of around 1.5 mm, in the context of an absorber, the composite demonstrated MW absorption for C radar range, while the thickness is 3.5 mm, it exhibited MW absorption in the Ku band.

Cao and colleagues fabricated ternary nanocomposites of MWCNTs/CoFe₂O₄/FeCo. The nanocomposite was coated with polyaniline using sol-gel in situ polymerization. The 1.5mm sample displayed a remarkable minimum reflection loss (RL) of approximately -90dB at 13.8GHz, with an effective bandwidth of 4GHz. These nanocomposites exhibited improved polarization at the interfaces, matching of impedance, and exchange coupling, resulting in exceptional microwave absorption properties. They proved to be excellent absorbers, featuring strong absorption, thin thickness, and the widest effective bandwidth.

Zhu and colleagues successfully fabricated ternary composites of MnFe₂O₄@SiO₂-Polyaniline-PVDF. A core-shell structure was created utilizing a straightforward approach at ambient temperature. The research results revealed that the composites containing 20wt% MnFe₂O₄@SiO₂ and 20wt% Polyaniline in the Polyvinylidene fluoride matrix displayed the most extraordinary performance. The minimum RL is -25.73dB at 12.32GHz, and the EAB spanned from 10.72 to 14.40GHz.

Xiong and his team developed a novel ternary composite of NiFe₂O₄@SiO₂/MWCNT. This composite exhibited exceptional absorbing performance due to the combined effect of dielectric loss, magnetic loss, and excellent impedance matching. The reflection loss (RL) of the composite was approximately -67.8dB when the thickness was 1.9mm. For a thickness of 1.5mm,

the effective absorption bandwidth (RL < -10dB) extended over 4.5GHz (from 13.5GHz to 18GHz). Similarly, for 2.2mm, the EAB reached 5.3GHz (in-between 12.7GHz to 18GHz).

Hosseini et al. synthesized core-shell nanocomposites of MnFe₂O₄/Fe₃O₄/polythiophene through a two-step co-precipitation method and in situ polymerization. The resulting nanocomposites displayed a core-shell structure with an average diameter ranging from 30 to 60 nm. The TEM images clearly showed the Fe₃O₄ coating on the surface of MnFe₂O₄. The nanocomposite demonstrated a lowest RL of -21 dB over a frequency of 12 GHz, with a thickness of 1.5 mm.

Wang and colleagues investigated the microwave absorption properties of Iron ferrite-Cobalt-porous carbon obtained through in situ thermally carbonizing in a N₂ environment, utilizing ferrite/ZIF-67. Among prepared samples, FC500, produced at 500°C, exhibited the most robust microwave absorption performance. At a thickness of 1.5 mm, FC500 demonstrated a minimum RL at 14.32 GHz of approximately -31.05 dB, with an EAB spanning 4.8 GHz (from 12.24 GHz to 17.04 GHz). The study findings indicate that a thin ternary absorbing material is optimal, leading to ferrite absorbing material with significant decreased weight.

2.16 Quaternary Ferrite Microwave Absorbing Nanocomposite

Yu-Lan and his team achieved a significant milestone by successfully synthesizing quaternary nanocomposites comprising graphene, Fe₃O₄@Fe core/shell nanoparticles, and ZnO nanoparticles. The electromagnetic parameters measured from these nanocomposites demonstrated their impressive performance. The absorption bandwidth, where the reflection loss is less than -20 dB, reached up to 7.3 GHz, and within this frequency range, over 99% of the electromagnetic wave energy was attenuated.

Yan and his team developed a quaternary composite of CuS/RGO/PANI/Fe₃O₄ and extensively investigated the impact of its unique microstructure on electromagnetic wave absorption performance. The measured results revealed that CuS/RGO/PANI/Fe₃O₄ exhibited remarkable microwave absorption capacity, surpassing that of CuS/RGO and CuS/RGO/PANI composites. The most significant reflection loss reached -60.2 dB at 10.2 GHz, and the absorption bandwidth below -10 dB spanned 7.4 GHz (ranging from 7.5 to 14.9 GHz) for a 2.5 mm coating thickness.

In their study, S.S. Afzali et al. investigated the microwave absorption characteristics of nanocomposites consisting of MWCNT/CuO/Fe₃O₄/Polyaniline. These nanocomposites were synthesized using three different weight ratios of CuO/Fe₃O₄/PANI to MWCNT (1:3, 1:4, and 1:5). Figure 37 illustrates the minimal reflection losses observed for the MWCNT/CuO/Fe₃O₄/PANI nanocomposites with weight ratios of (1:3), (1:4), and (1:5), which were 45.7 dB, 58.7 dB, and 85.4 dB, respectively.

In conclusion, the quaternary nanocomposite absorbing material exhibits significantly enhanced microwave absorption performance compared to binary or ternary nanocomposites. This improvement is achieved through the synergistic impact of dielectric loss, magnetic loss, and impedance matching, along with the special hierarchical nanostructure that integrates distinct microwave loss mechanisms of each component. However, it is important to consider that the preparation process for quaternary composites is more complex, necessitating careful attention to the binding and matching of each component.

The review above highlights the promising future of quaternary hybrid nanocomposites in advancing stealth technology, offering strong absorption and wide frequency capabilities.

Chapter 3

Experimental and Characterization

3.1 Materials

Ammonium iron (III) sulphate dodecahydrate $((\text{NH}_4)\text{Fe}(\text{SO}_4)_2 \cdot 12\text{H}_2\text{O})$, Reagent Plus, × ; ; ' . " Argonmium-iron"(II) sulphate hexahydrate $((\text{NH}_4)_2\text{Fe}(\text{SO}_4)_2 \cdot 6\text{H}_2\text{O})$, T g c i g p v " R n w u . manganese(II) sulfate monohydrate" $(\text{MnSO}_4 \cdot \text{H}_2\text{O})$, T g c i g p v " R n w u . " × ; ; ' . " O g t e m + . $3)_2$ e 6H₂O, ACS" p k v t c reagent, × ; : ' " O g t e m + " c o o q p h k 35%, u A R f o w A n a l y s i s , ' F i s h e r J Chemicals), u q f k w o " j { f t q z k f g " * P c Q J . " r g n n g v u . " c p Merck), sulfuric acid (H_2SO_4 , ACS reagent, 95% - 98%, Merck), nitric acid (HNO_3 , 65%, EMPLURA, Merck), hydrazine monohydrate ($\text{N}_2\text{H}_4 \cdot \text{H}_2\text{O}$, reagent grade, 98%, Merck), ethylene glycol ($\text{C}_2\text{H}_6\text{O}_2$, anhydrous, 99.8%, Merck) were used as received without any additional steps for purification.

3.2 Synthesis of Nanocomposite

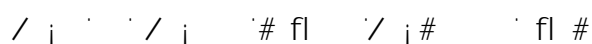
3.2.1 Functionalization of multi-walled Carbon nanotubes (MWCNTs)

Multi-walled carbon nanotubes with diameter of 10-20 nm, length up to μm were used. The as received MWCNTs have no surface charged functional group on them. The carbon atoms are strongly covalent bonded with no interaction with other species. By functionalizing the surfaces of CNTs with negatively charged functional groups (MWCNTs-COOH), these can be used for further applications.

Functionalization of MWCNTs was done by thermal oxidation. One gram of as-received MWCNTs was added to a 50 ml solution of concentrated nitric and sulfuric acid in a ratio of 1:3 (v/v). The mixture was dispersed using a bath sonicator for 1 hour at room temperature. The solution was then refluxed under magnetic stirring at 80°C for 6 hours. After cooling the mixture to room temperature, the mixture is diluted with excess deionized water followed by centrifugation at 8000 rpm for 10 minutes. The washing process is repeated until the pH of MWCNTs reaches around 7. Subsequently, the material is dried in a vacuum oven at 100°C . The final solid dry MWCNTs are grinded into fine powder by mortar pestle.

3.2.2 Synthesis of MWCNTs óIron Ferrite Nanocomposite (MWCNTs-Fe₃O₄)

The growth of ferrite nanoparticles on MWCNTs' surface followed a co-precipitation route. A solution of Fe⁺² salt and Fe⁺³ salt were prepared in 200ml deionized water with Fe⁺²:Fe⁺³=1:2. In the above solution, the oxidized MWCNTs were sonicated for half an hour. The mass ratio of MWCNTs : Fe⁺² + Fe⁺³ should be 1:1. The solution was placed in a water bath and heated up to 50°C. 8M NH₄OH solution was added drop wise in the above mixture with constant stirring until the pH of the solution becomes 12. The solution is further stirred and heated at 50°C for 2 hours to complete the growth of nanoparticles. The co-precipitation reaction for growth of Fe₃O₄ is



The MWCNTs - Fe₃O₄ nanocomposite was separated by a strong magnet. The nanocomposite is washed several times with deionized water and ethanol until pH becomes normalized. After washing, the nanocomposite was dried at 60°C in a vacuum oven. The mass ratio is between MWCNTs and Fe⁺² + Fe⁺³ is varied as (1:1/2, 1:1/3, 1:1/4, 1:1/5, 1:1/6) to obtain MWCNTs with different loading of Fe₃O₄ nanoparticles. These samples are denoted as CF1, CF2, CF3, CF4, CF5, CF6. Similar procedure is adapted to synthesis Fe₃O₄ nanoparticles without MWCNTs.

3.2.3 Synthesis of MWCNTs óManganese Ferrite Nanocomposite (MWCNTs-MnFe₂O₄)

The reaction procedure for synthesis of MWCNTs-MnFe₂O₄ is same as above. A solution is prepared in 200ml deionized water of Mn⁺² and Fe⁺³ salts with Mn⁺² : Fe⁺³ = 1:2. The solution is sonicated with MWCNTs (MWCNTs : Mn⁺² + Fe⁺³ = 1:1) for half hour. Subsequently, the mixture was heated in a water bath, gradually raising the temperature to 50°C.. Ammonia solution (8M) is added drop wise with constant stirring till pH reaches 11-12. Afterwards, the solution is kept at 50°C for 2 hours with constant stirring. The precipitation reaction is



The obtained MWCNTs-MnFe₂O₄ was not attracted by a magnet. Subsequently, the sample was subjected to vacuum filtration using a filter paper of pore size 3 µm. It

was then thoroughly washed with deionized water and ethanol. After the washing process, the sample was dried in a vacuum oven at 60°C. A pellet of sample was prepared and sealed in a quartz tube with a vacuum of 10⁻² mbar. The sample was annealed at 800°C for 2 hours. After reaching at room temperature, the pellet was removed from vacuum tube and grinded into fine powder with mortar pestle. The mass ratio is between MWCNTs and Mn⁺² + Fe⁺³ is varied as (1:1/2, 1:1/3, 1:1/4, 1:1/5, 1:1/6) to obtain MWCNTs with different loading of MnFe₂O₄ nanoparticles. These samples are denoted as CM1, CM2, CM3, CM4, CM5, CM6. Similarly, the MnFe₂O₄ nanoparticles are synthesized without addition of MWCNTs.

3.2.4 Synthesis of MWCNTs óCobalt Nanocomposite (MWCNTs-Co)

MWCNTs óCobalt nanocomposite was prepared by reduction in hydrazine-alkaline system. An appropriate amount of Co⁺² salt is dissolved in 50 ml ethylene glycol. The MWCNTs were sonicated in the solution mentioned above using probe sonication for duration of half an hour. The mass ratio between MWCNTs and Co⁺² is 1:10. NaOH (2.5 M) is then added in the above solution. The solution is heated and stirred in a water bath at 80°C. A solution of hydrazine and ethylene glycol was added drop wise in the above solution. All Co⁺² ion are allowed to precipitate in the solution by keep heating at 80°C for 60 minutes. The precipitation reaction is as follows



The nanocomposite is collected by a strong magnet and then washed with ethanol until pH is normalized. The collected sample is dried under vacuum at room temperature. The mass ratio is between MWCNTs and Co⁺² is varied as (1:5, 1:2.5, 1:1.25, 1:0.6, 1:0.3) to obtain MWCNTs with different loading of Co nanoparticles. These samples are denoted as CC1, CC2, CC3, CC3, CC5, CC6. Cobalt nanoparticles are also prepared from the same synthesis reaction.

3.2.5 Synthesis of MWCNTs óManganese Ferrite óIron Ferrite - Cobalt hybrid Nanocomposite (MWCNTs - MnFe₂O₄ - Fe₃O₄ - Co)

The hybrid nanocomposite is prepared by the synthesis procedure discussed above. Initially, MnFe₂O₄ are precipitated, as the synthesis required high temperature annealing. Afterwards, Fe₃O₄ are grown on the surface of MWCNTs - MnFe₂O₄.

Finally, Co nanoparticles are reduced on the surface of MWCNTs - MnFe₂O₄ - Fe₃O₄ nanocomposite. The mass ratio of MWCNTs, Mn⁺² + Fe⁺³, Fe⁺² + Fe⁺³, and Co⁺² is (1:1/5:1/5:0.6).

3.3 Characterization Techniques

3.3.1 Scanning Electron microscopy (Size and morphology)

The morphology and particle size of all synthesized nanomaterials was studied in a JEOL JSM-6490A (JEOL, USA, Inc.) scanning electron microscope (SEM). A suspension each sample of nanocomposite was prepared by dispersing small quantity of dry powder in absolute ethanol using a probe sonicator (Sonics Vibra VC750, Newtown, CT, USA). A fractional quantity of each diluted suspension was deposited onto a glass slide and allowed to undergo evaporation under ambient conditions. The determination of the size and its distribution of the produced nanomaterial involved measuring the individual size of 100 particles and afterwards creating a histogram using Image-J software.

The energy-dispersive X-ray detector (EDX) was used to determine the elemental composition of the substance.

3.3.2 X-ray Diffraction (Crystallographic analysis)

The phase and structure of synthesized nanomaterial were analyzed by X-ray diffraction (XRD, GNR, Explorer, Italy). The powder samples' patterns were recorded at room temperature by using a Bruker D8 Advance X-ray diffractometer with a Cu K α radiation (35 kV and 45mA). The XRD patterns were scanned in the range of 20° and 80° with a step increment of 0.01°.

The average size of the crystallite was calculated using the Scherrer equation:

$$D = \frac{0.9 \lambda}{\Delta 2\theta \cos \theta}$$
 where D is the average crystallite size, λ is the wavelength of the X-ray (0.154 nm), $\Delta 2\theta$ is the full width at half maximum (FWHM) of the diffraction peak, and θ is the Bragg angle.

3.3.3 Vibrating Sample Magnetometer (Magnetic hysteresis measurement)

The magnetic hysteresis of all nanocomposites was determined using a vibrating sample magnetometer (VSM, Lakeshore 8600, Westerville, OH, USA). The measurements were performed at room temperature by subjecting the dry powder sample, placed in a plastic sample holder, to an external magnetic field to generate the hysteresis curves..

3.3.4 Thermogravimetric analysis

The content of magnetic phase in the CNTs nanocomposite is determined by thermogravimetric analysis (TGA). The measurement involves recording the changes in mass with respect to temperature. The thermogravimetric analysis of powder samples were investigated with a thermal analysis system (TGA/DSC 1, Mettler Toledo, USA) in air with a heating rate of 12°C/min from 30°C to 850°C.

3.3.5 Fourier transformed Infrared spectroscopy

FTIR spectroscopy was carried out using a JASCO-FT/IR-6800 spectrophotometer (Hachioji, Tokyo, Japan) covering the wavenumber range from 4000 to 300 cm⁻¹.

3.3.6 Raman Spectroscopy

Raman spectra measurements on powdered samples were performed on an iRaman BWS415-532S (B&W Tek, Newark, NJ, USA) portable spectrometer system. The samples were excited by using a near-infrared laser diode having a wavelength of 532nm and maximum laser output of 60mW. All the spectra were recorded on a peltier cooled linear CCD array detector.

3.3.7 Microwave Absorption

Microwave absorption was measured in the range of 1-20 GHz range by using a network analyzer (Anritsu MS46122B) with coaxial waveguide method. The sample was mixed with melted paraffin wax with a ratio of 10%. The mixture was compressed into a ring of inner diameter 2.95 mm, outer diameter 6.1 mm and thickness of 1 mm.

Chapter 4

Results and Discussion

4.1 Raman Spectroscopy

The Raman spectroscopy is employed to investigate the effect of functionalization on MWCNTs by analyzing the attachment of functional groups. Figure A illustrates the Raman spectra of both pristine and functionalized MWCNTs. In both cases, characteristic bands of CNTs are observed, including the G-band around 1530 cm^{-1} , the D-band around 1350 cm^{-1} , and the G' band (D overtone) around 2700 cm^{-1} . The G-band arises from in-plane or tangential vibration of carbon atoms, involving bending and stretching of sp^2 carbon-carbon bonds in the C-plane of graphite. On the other hand, the D-band originates from structural disorders in the carbon nanostructures. It represents collective in-plane vibrations towards and away from the ring center formed by sp^2 bonded carbon atoms.

The ID/IG intensity ratio directly correlates with the quantity of surface defects and sp^3 -hybridized carbon atoms present in a CNT, thereby providing valuable information about the extent of sidewall functionalization. The ID/IG ratio represents the degree of crystallinity in the CNT sample..

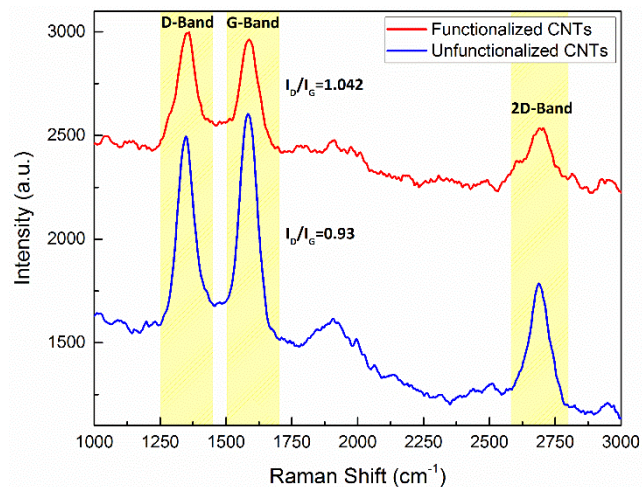


Figure 1 Raman Spectra of Unfunctionalized and Functionalized MWCNTs

The value of I_D/I_G measured from the spectra of pristine MWCNTs is 0.93 and functionalized MWCNTs is 1.042. The increase in I_D/I_G ratio after functionalization indicates new defects in MWCNTs geometry by successful binding of functional group on the surface of MWCNTs. The modification process involves two steps: opening of tube caps and formation of functional groups at the side walls.

The slight difference in I_D/I_G values between pristine and functionalized MWCNTs indicates that the overall structure of the CNTs was preserved after functionalization. Harsh oxidation conditions can potentially damage the MWCNT structure and reduce their reinforcing ability in nanocomposites. However, our functionalization procedure was designed to create the desired functional groups while maintaining the integrity of the MWCNT structure to minimize the risk of tube shortening.

4.2 X-ray Diffraction

4.2.1 XRD of MWCNTs óIron Ferrite Nanocomposite (MWCNTs-Fe₃O₄)

The figure shows the XRD pattern of functionalized MWCNTs (a), Fe₃O₄ (b) and MWCNTs- Fe₃O₄ (c). From figure (a), the sharp diffraction peaks at 25.5° indexed as (002) plane and peak at 42.4° indexed as (100) plane corresponds to characteristic peaks of MWCNTs (JCPDS No. 96-101-1061). The figure (b) shows the diffraction of synthesized Fe₃O₄ nanoparticles. The diffraction peaks in the pattern appeared at 30.0°,

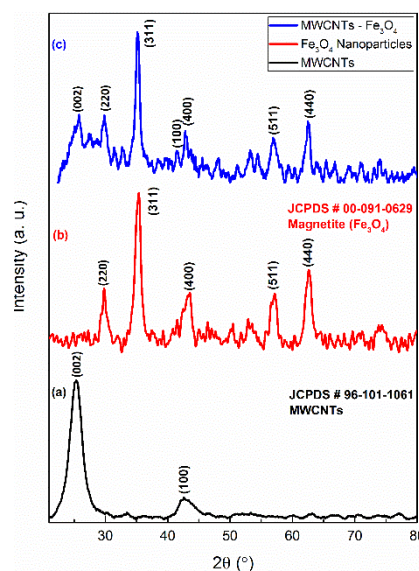


Figure 2 XRD pattern of MWCNTs, Fe₃O₄ and MWCNTs-Fe₃O₄ nanocomposite

35.5°, 43.1°, 57.0, 62.7° corresponds to the crystallographic planes (220), (311), (400), (511), (440) respectively. These peaks correspond to formation of magnetite nanoparticle with cubic inverse spinel structure (JCPDS No. 00-091-0629). Magnetite is a type of iron oxide with a mixed valence, consisting of Fe⁺² and Fe⁺³ ions, arranged in an inverse spinel structure. Within each unit cell of magnetite, there are eight tetrahedral interstitial sites occupied by Fe⁺³ ions, along with an additional sixteen octahedral interstitial sites that are shared between eight Fe⁺³ and eight Fe⁺² ions. Additionally, there are 32 oxygen ions situated in closely packed planes throughout the structure.

For figure (c), the diffraction pattern of nanocomposite distinctly coincides with both diffraction pattern of MWCNTs and cubic inverse spinel structure of magnetite nanoparticle, indicating the formation of MWCNTs- Fe₃O₄ nanocomposite.

4.2.2 XRD of MWCNTs óManganese Ferrite Nanocomposite (MWCNTs- MnFe₂O₄)

The XRD patterns of functionalized MWCNTs (a), MnFe₂O₄ (b), and MWCNTs- MnFe₂O₄ before (c) and after annealing (d) are shown in figure. In the XRD pattern of synthesized MnFe₂O₄ nanoparticles (b), the peaks at 30.1°, 35.40°, 43.14°, 53.30°, 56.88°, and 62.33° which correspond to (2 2 0), (3 1 1), (2 2 2), (4 0 0), (4 2 2),

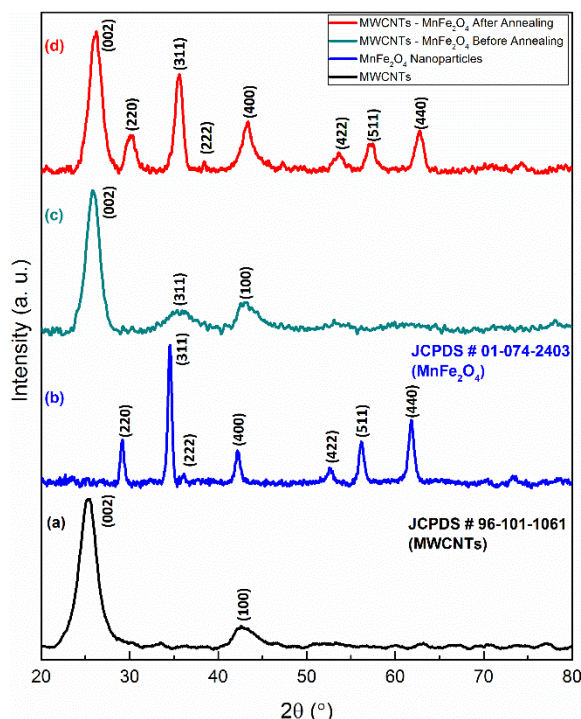


Figure 3 XRD pattern of MWCNTs, MnFe₂O₄, MWCNTs-MnFe₂O₄ nanocomposite before and after annealing

(5 1 1), and (4 4 0) diffraction planes of the $MnFe_2O_4$ phase matched the standard values in JCPDS card no. 10-0319, confirming the face-centered cubic spinel of jacobsite ferrite and its space group to $Fd3m$. In the XRD pattern of MWCNTs- $MnFe_2O_4$ before annealing, the peaks of MWCNTs and a single peak of $MnFe_2O_4$ appeared at 35.40 corresponding to (311) plane. This shows that the synthesized $MnFe_2O_4$ in the nanocomposite is not in a complete crystalline phase during the synthesis. After annealing, the sample shows all the characteristics XRD peaks of both MWCNTS and $MnFe_2O_4$. This confirms the formation of well-defined single phase cubic spinel structure. The (111) plane overlaps with the (400) that of CNT. No peaks were observed corresponding to formation of manganese oxide and/ or iron oxide. These peaks precisely coincide with both patterns i-e of MWCNTs and $MnFe_2O_4$ nanoparticle, indicating the formation of MWCNTs- $MnFe_2O_4$ nanocomposite.

4.2.3 XRD of MWCNTs óCobalt Nanocomposite (MWCNTs-Co)

The XRD patterns shown in figure are MWCNTs (a), Co nanoparticles (b) and MWCNTs-Co nanocomposite (c). The diffraction pattern (b) shows multiple peaks at

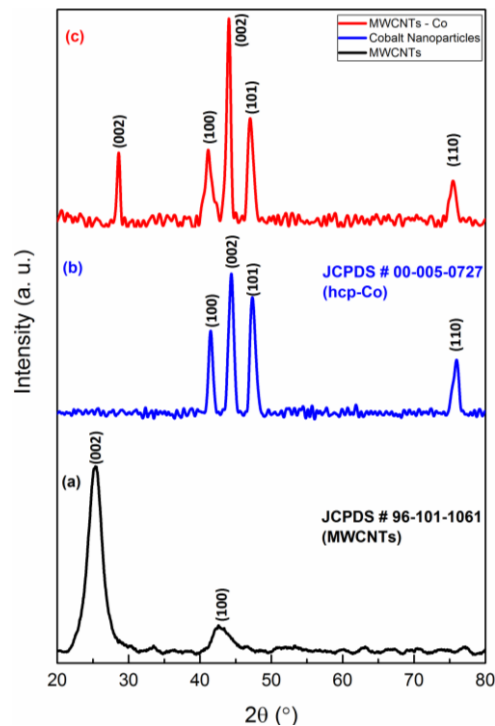


Figure 4 XRD pattern of MWCNTs, Co and MWCNTs-Co nanocomposite

41.5°, 44.5°, 47.3° and 75.9° attributed to hexagonal structure of metallic with diffraction planes (100) (200) (101) and (110) respectively.

No characteristic peaks for impurities are detected indicating formation of pure metallic hexagonal Cobalt nanoparticles. The diffraction pattern (c) is the combination of diffraction pattern of MWCNTs and Co, which confirms the formation of desired nanocomposite. The average crystallite size of the synthesized nanoparticles was determined using Scherrer's formula, based on the characteristic high intensity peaks of each sample. The obtained values are listed in the table 1.

Table 1 Crystallite size of Fe₃O₄, MnFe₂O₄, Co nanoparticles attached with MWCNTs measured from Scherrer formula

Nanocomposite	Plane	2θ (°)	FWHM	Crystallite Size d (nm)
MWCNTs-Fe ₃ O ₄	(311)	35.54413	0.72816	12 ± 2
MWCNTs-MnFe ₂ O ₄	(311)	35.6203	1.04499	10 ± 2
MWCNTs-Co	(002)	44.54695	0.55104	16 ± 2

4.3 Thermogravimetric analysis

4.3.1 TGA of MWCNTs-Iron Ferrite Nanocomposite (MWCNTs-Fe₃O₄)

The quantities of Fe₃O₄ in the different composition of synthesized MWCNTs-Fe₃O₄ nanocomposite are estimated by TGA in air shown in figure. The TGA curve of nanocomposite shows same decomposition behavior as that of MWCNTs. The initial weight loss in the functionalized MWCNTs curve was due to elimination of surface functional group i.e. -OH, -COOH. This is followed by a huge weight loss which occurs till ~600°C is related to the oxidation of MWCNTs to CO₂. After 600°C, all of the MWCNTs were decomposed to CO₂ and the residue corresponds to the mass fraction of nanoparticles attached to the surface of MWCNTs.

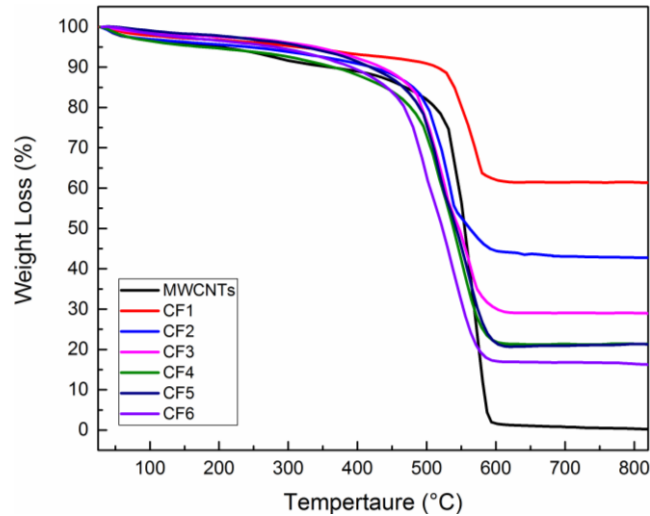


Figure 5 TGA curve of different concentration of MWCNTs-Fe₃O₄ nanocomposite

In case of MWCNTs-Fe₃O₄, the final residue corresponds to Fe₂O₃, due to oxidation of Fe₃O₄.

From the residual weight of Fe₂O₃ and the above oxidation reaction, the weight percent of Fe₃O₃ is calculated. The weight percent loading of nanoparticles in each nanocomposite is given in the table.

4.3.2 TGA of MWCNTs óManganese Ferrite Nanocomposite (MWCNTs-MnFe₂O₄)

In case of MWCNTs-MnFe₂O₄ nanocomposite, the comparison of TGA curves with decomposition of MWCNTs in air is shown in figure. Similar decomposition behavior of MWCNTs and nanocomposites can be observed. The final residues, after oxidation of MWCNTs around 600°C, are Mn₂O₃ and Fe₂O₃. This residual weight of MnFe₂O₄ corresponds to oxidation of Mn(II) to Mn(IV).

According to the residual weight percent of nanocomposites and above oxidation reaction, the weight percentages of $MnFe_2O_4$ in the nanocomposites are calculated and given in the table.

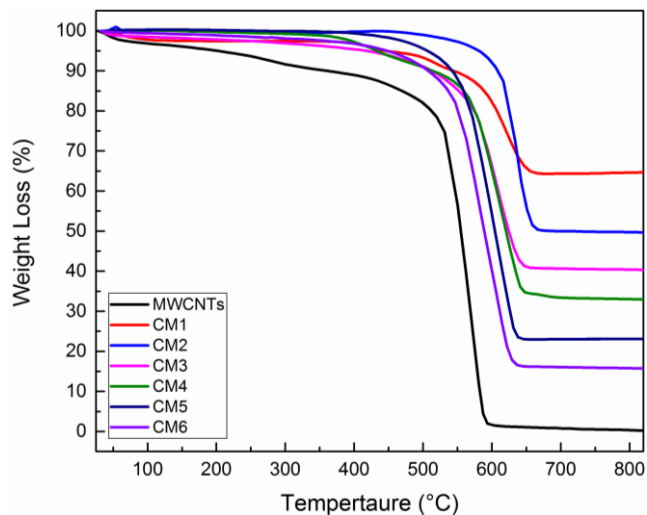


Figure 6 TGA curve of different concentration of MWCNTs- $MnFe_2O_4$ nanocomposite

4.3.3 TGA of MWCNTs óCobalt Nanocomposite (MWCNTs-Co)

The TGA curves of nanocomposite with varying amount of Co and MWCNTs are shown in figure. The decomposition of nanocomposite is analogous to that of MWCNTs with major weight loss due to oxidation of MWCNTs to CO_2 . According to the reaction below, the residue obtain corresponds to Co_3O_4

From the residual weight and above reaction the wt% of the Cobalt in the nanocomposite is estimated and given in the table.

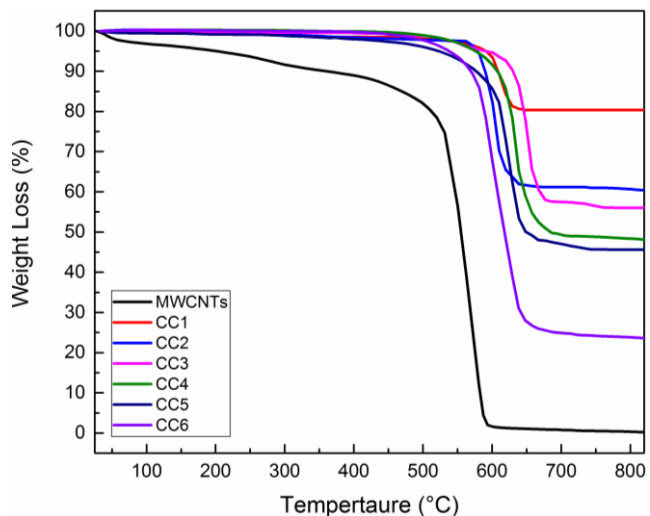


Figure 7 TGA curve of different concentration of MWCNTs-Co nanocomposite

The TGA of the nanocomposite, having a varying amount of nanoparticles attached MWCNTs, showed that the composition estimated during synthesis matches the results obtained via TGA. This indicates that the method reported is capable of exactly tailoring the composition of MWCNTs nanocomposite.

Table 2 The percentage loading of nanoparticles on the surface of MWCNTs calculated from TGA decomposition curves

Description	Weight Percent Loading of Nanoparticles		
	Fe ₃ O ₄	MnFe ₂ O ₄	Co
CF1/ CM1/ CC1	64	64	68
CF2/ CM2/ CC2	44	49	51
CF3/ CM3/ CC3	30	40	47
CF4/ CM4/ CC4	22	32	40
CF5/ CM5/ CC5	21	23	38
CF6/ CM6/ CC6	17	15	19

4.4 Morphological Study

4.4.1 Unfunctionalized and Functionalized CNTs

Surface morphology was examined of the as received MWCNTs (unfunctionalized) and acid treated MWCNTs (functionalized). The figure 1a shows the surface of unfunctionalized MWCNTs, which shows an equal size distribution of MWCNTs in the entire sample. Moreover, the surface of the unfunctionalized MWCNTs is very smooth, indicating no surface defects. The average size estimated of these unfunctionalized MWCNTs is 40 ± 10 nm. Figure 1b illustrate that the tube structure of MWCNTs with similar length was preserved after treatment with acid. However, the surface of functionalized MWCNTs appears to be rougher. This indicates that the acid treatment did not damage the structure of the MWCNTs but imparted defects on the surface of the functionalized MWCNTs in the form of carboxylic and hydroxyl functional groups. This is also evident from the size increase of functionalized MWCNTs. The average size measure of functionalized MWCNTs is 45 ± 10 nm.

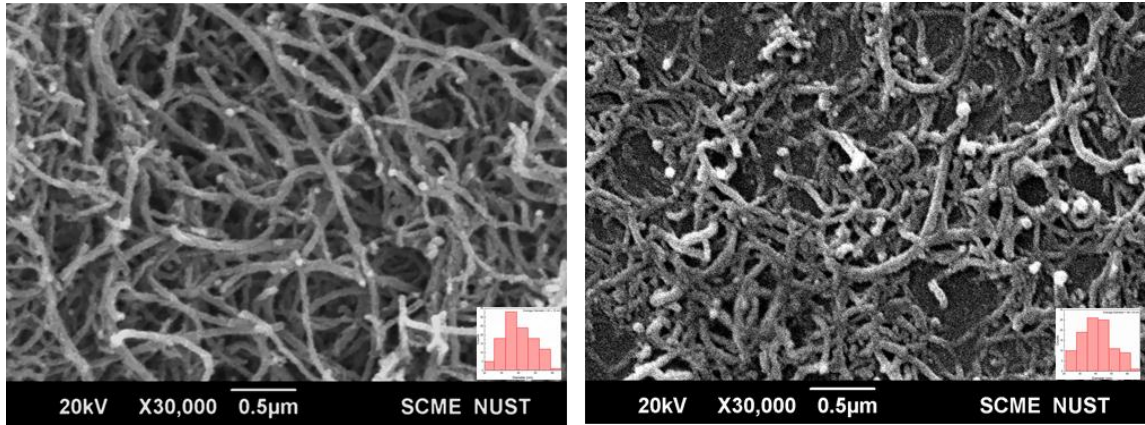


Figure 8 SEM images of (a) Unfunctionalized MWCNTs (b) Functionalized MWCNTs

4.4.2 MWCNTs óIron Ferrite Nanocomposite (MWCNTs-Fe₃O₄)

The figure 2 shows the SEM images of MWCNTs-Fe₃O₄ synthesized nanocomposite with different loading of Fe₃O₄. All the images show the tubular structure of MWCNTs is intact after the in-situ growth of Fe₃O₄ nanoparticles. The figure 2a shows the

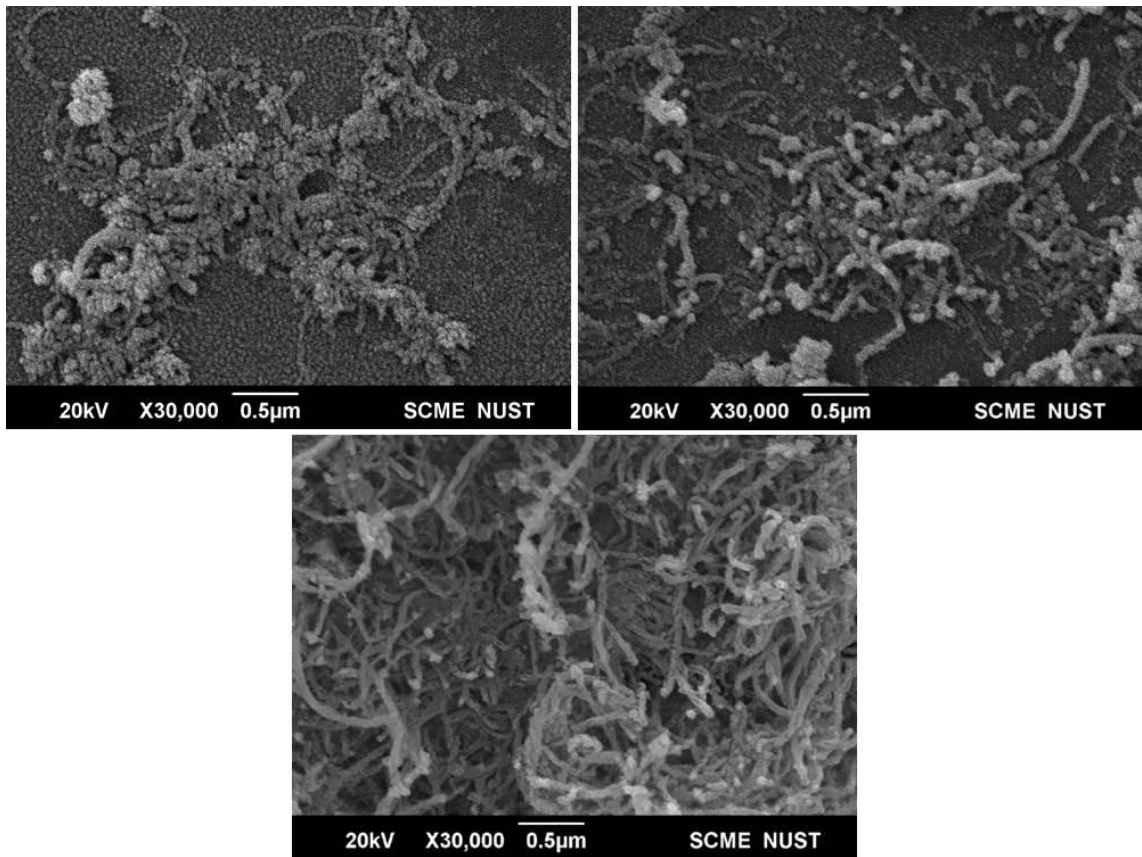


Figure 9 SEM images of MWCNTs-Fe₃O₄ nanocomposite (a) 62% loading (b) 42% loading (c) 20% loading

MWCNTs-Fe₃O₄ nanocomposite with 62% loading. The high loading is evident from the figure. The particles are agglomerated on the surface of MWCNTs and also present on the surface of the sample holder. The MWCNTs are overloaded with Fe₃O₄ nanoparticles. Only the particles on the surface of the MWCNTs are chemically attached and further particles are adsorbed on the surface. This is evident that due to prolong sonication the adsorbed Fe₃O₄ nanoparticles were detached. The figure 2b shows nanocomposite with 42% loading. The nanoparticles have completely covered the surface of MWCNTs and very small agglomeration is seen on the surface. The figure 2c shows nanocomposite with only 20% loading. The low loading is evident from the figure, as most of surface of MWCNTs is without any Fe₃O₄ nanoparticles. The remaining surface can further be utilized for growth of other nanoparticles. The particles size of Fe₃O₄ is measured to be 20 ± 5 nm.

4.4.3 Manganese Ferrite Nanocomposite (MWCNTs-MnFe₂O₄)

The figure 3 depicts the morphology of MWCNTs-MnFe₂O₄ nanocomposite synthesized. The MWCNTs act as a substrate for nucleation of nanoparticles growth.

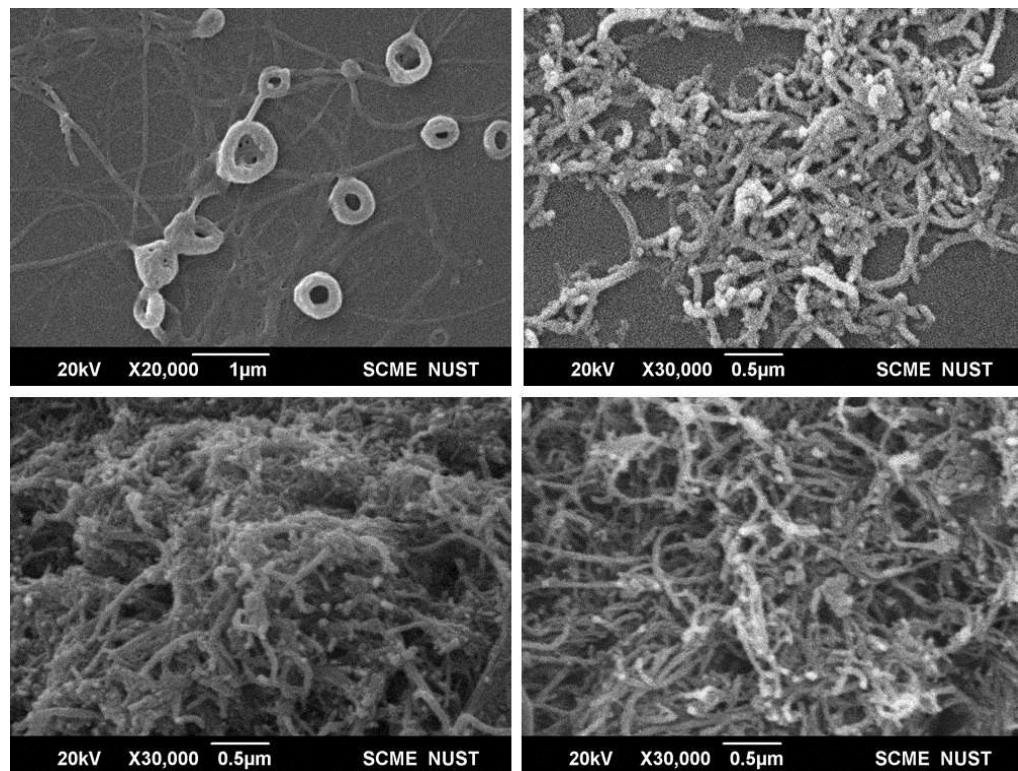


Figure 10 SEM images of MWCNTs-MnFe₂O₄ nanocomposite (a) 29% loading before annealing (b) 29% loading after annealing (c) 40% loading after annealing (d) 16% loading after annealing

The structure of MWCNTs is intact, revealing that the structure is not damaged during synthesis. The figure 3a shows the SEM image of as synthesized MWCNTs-MnFe₂O₄ nanocomposite (before annealing). A donut like structure of MnFe₂O₄ nanoparticles is obtained. However, the sample before annealing did not show any magnetic behavior. From figure 3b, after subjecting to annealing the morphology of the MnFe₂O₄ change into particle like structure with mean size of 15 ± 5 nm. This morphology of MnFe₂O₄ nanoparticles are more magnetic as revealed by VSM (discussed later). The figure 3b, 3c, 3d represents the nanocomposite with 29%, 40%, 16% loading. The figure 3d illustrate that the surface of MWCNTs is not completely covered with MnFe₂O₄ nanoparticles and site for further nucleation is available for different nanoparticles in-situ growth.

4.4.4 MWCNTs óCobalt Nanocomposite (MWCNTs-Co)

The figure 4 represents the MWCNTs-Co nanocomposite synthesized. The observed

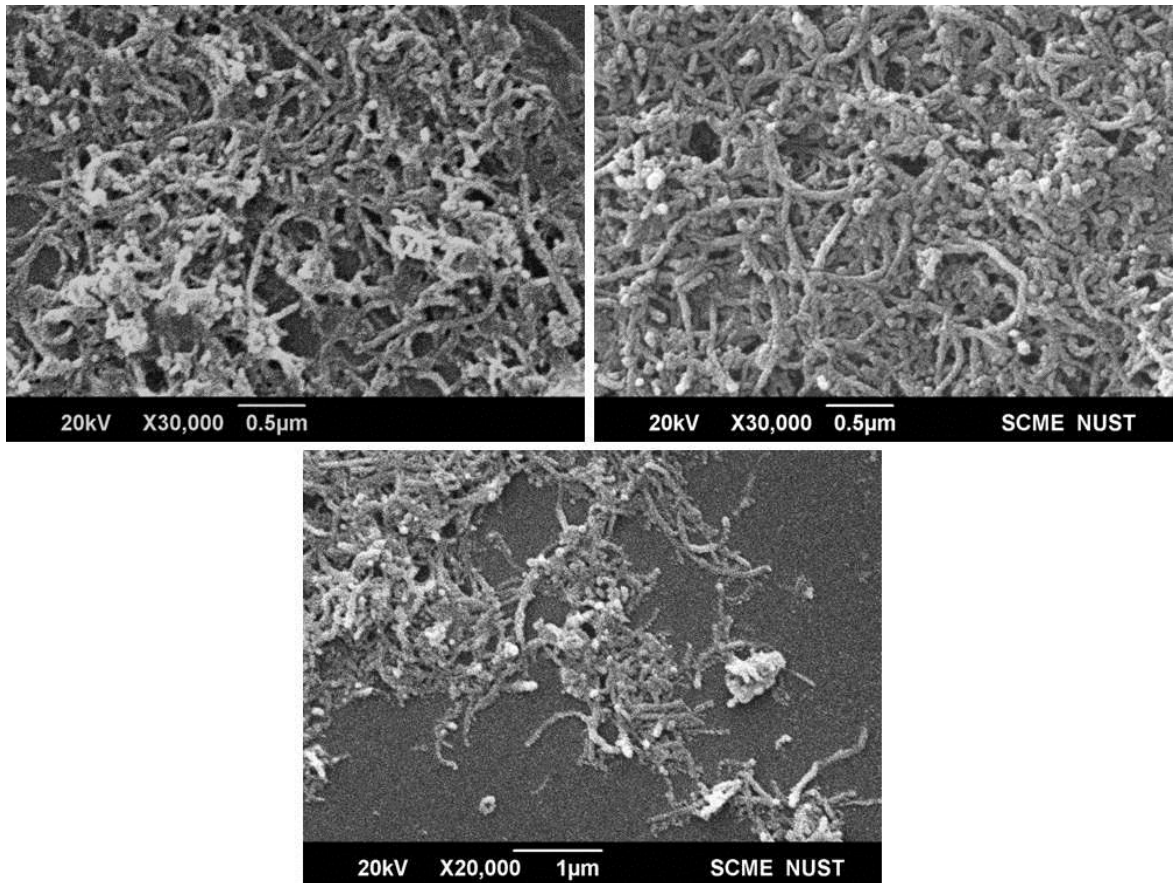


Figure 11 SEM Images of MWCNTs-Co nanocomposite (a) 68% loading (b) 51% loading (c) 38% loading

morphology of tube structure of MWCNTs shows no damage during synthesis and particle like morphology of Co nanoparticles in all nanocomposite samples. All SEM images show successful attached of Co nanoparticles with MWCNTs. The figure 4a represents 68% loading of Co nanoparticles on the surface. The high loading of particles results in agglomeration of nanocomposite. Similarly, the figure 4b represents the nanocomposite with 51% loading. The particles are uniformly distributed on the surface of MWCNTs. Figure 4c illustrate 38% loading, revealing partial coverage of MWCNTs surface with Co nanoparticles. The functional group on the surface of MWCNTs acts as a nucleation site for nanoparticle growth. This causes a decrease in agglomeration and facilitates smaller particle size. The size measure of Co nanoparticles is 10 ± 5 nm.

These SEM images show successful synthesis of MWCNTs nanocomposite with different magnetic nanoparticle with varying loading and small particle size. All of these factors contribute in large number of magnetic nanoparticles of MWCNTs having more surface area resulting in natural resonance, interface polarization and dipolar polarization for enhanced microwave absorption properties.

4.5 Magnetic Properties

4.5.1 Magnetic Properties of MWCNTs óIron Ferrite Nanocomposite (MWCNTs-Fe₃O₄)

The figure shows the magnetic hysteresis curves of MWCNTs-Fe₃O₄ nanocomposite at room temperature. The hysteresis curve of MWCNTs shows non-

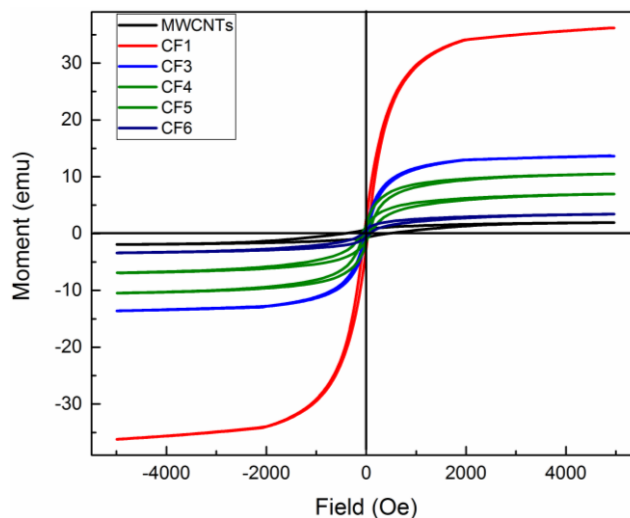


Figure 12 M-H hysteresis curves of MWCNTs and MWCNTs-Fe₃O₄ nanocomposite

magnetic behavior. The saturation magnetization (M_s) of MWCNTs is 1.9231 emu/g, with coercivity (H_c) of 431.49 Oe and remanence magnetization (M_r) of 0.69945 emu/g. The magnetic properties of the MWCNTs-Fe₃O₄ nanocomposite depend on the concentration of attached Fe₃O₄ nanoparticles. An increase in the ferrite content leads to a higher M_s value and a decrease in coercivity (H_c). The diamagnetic behavior of MWCNTs shifts towards super-thin hysteresis, indicating superparamagnetic behavior as the wt.% of Fe₃O₄ increases. The magnetic properties of the nanocomposite are primarily influenced by the ferrite nanoparticles. However, the M_s value of the nanocomposite with the highest ferrite content is lower than that of the Fe₃O₄ nanoparticles. This reduction is attributed to the non-collinearity of magnetic domains at the surface of Fe₃O₄ nanoparticles attached to MWCNTs, resulting in surface spin disorder and spin canting effects. The high M_s values in the nanocomposite may contribute to enhanced magnetic loss, which leads to increased absorption of the magnetic field associated with microwaves.

4.5.2 Magnetic Properties of MWCNTs óManganese Ferrite Nanocomposite (MWCNTs-MnFe₂O₄)

Magnetic characteristics of the MWCNTs-MnFe₂O₄ nanocomposite were examined at room temperature, and M-H hysteresis curves were generated up to 5 kOe. The hysteresis curve for the MWCNTs-MnFe₂O₄ nanocomposite was compared before and after annealing, and the results are represented in the figure. Following the annealing process, the saturation magnetization (M_s) value increased significantly from 1.23 emu/g to 11.7 emu/g, while the coercivity (H_c) decreased from 320 Oe to 156.61 Oe. This observed enhancement in M_s and reduction in H_c can be attributed to the high degree of crystalline structure and the increased particle size resulting from the annealing process, which leads to reduced surface spin canting. Controlling the coercivity of spinel ferrite nanoparticles involves various factors, including strain, inter-particle contact, grain size, and shape. The size of the nanoparticles has a particularly noteworthy impact on the M_s value. Smaller particles have a higher surface-to-volume ratio, which causes canted spins on their surfaces. Consequently, the saturation

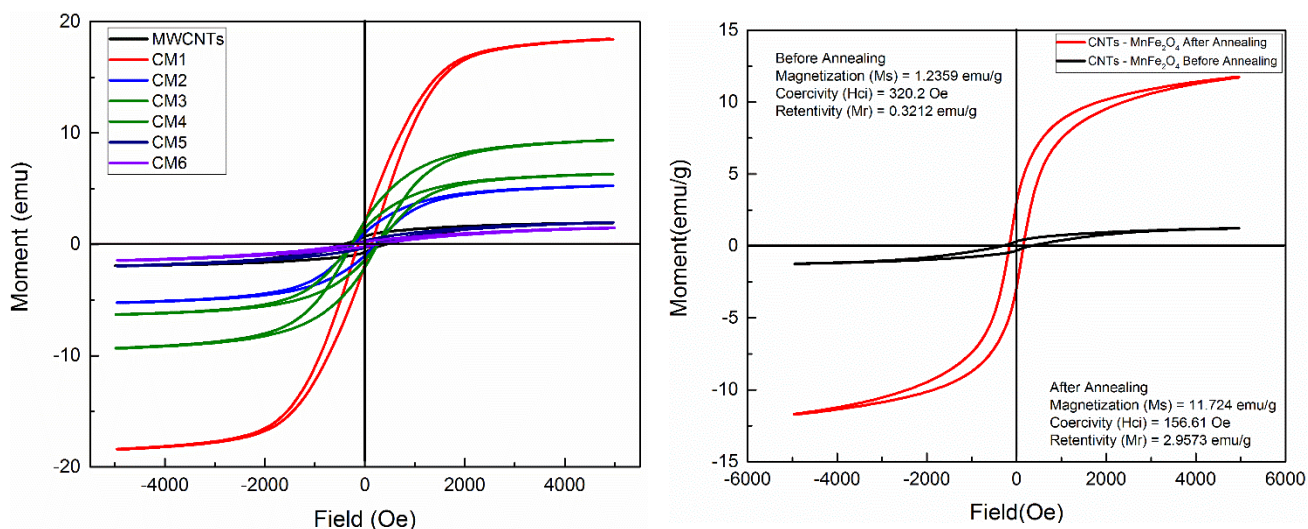


Figure 13 M-H hysteresis curves of MWCNTs and MWCNTs-MnFe₂O₄ nanocomposite (a) all concentration after annealing (b) 29% loading before and after annealing

magnetization of the sample diminishes, and the ferromagnetic core of the nanoparticle becomes more restricted in aligning with the direction of the applied magnetic field.

The figure presents a comparison between pure MWCNTs and the MWCNTs-MnFe₂O₄ nanocomposite with varying proportions of MnFe₂O₄. As the content of MnFe₂O₄ increases, both the M_s and H_c of the nanocomposite exhibit significant increments. This rise in MnFe₂O₄ concentration weakens the diamagnetic behavior of MWCNTs, leading to a shift towards superparamagnetic characteristics with lower H_c values.

Despite the observed increase, the M_s value in the MWCNTs- MnFe₂O₄ nanocomposite remains lower than the theoretically expected M_s value for MnFe₂O₄ nanoparticles, which is 80 emu/g. The decrease in M_s value in the nanocomposite is ascribed to typical surface disorder in spin and canting effect associated with superparamagnetic particle magnetization. In this case, the magnetic moments align with the applied field but deviate when the field is removed due to thermal energy. The presence of non-magnetic MWCNTs causes a significant disordered surface spin layer and polar interaction at the interface between the two phases, resulting in lower M_s values for samples with higher MWCNT concentrations.

4.5.3 Magnetic Properties of MWCNTs óCobalt Nanocomposite (MWCNTs-Co)

The figure displays the magnetic hysteresis (M-H) profiles of the MWCNTs-Co nanocomposite, showcasing its magnetic characteristics at room temperature. All the composites demonstrate an increase in magnetization as the magnetic field is raised, indicating the magnetic activity of the Co nanoparticles connected to the MWCNTs.

The rise in M_s (saturation magnetization) value is directly influenced by the quantity of Co nanoparticles present in the nanocomposite. It is worth noting that the coercivity measurements of the nanocomposite surpass the bulk value of 100 Oe,

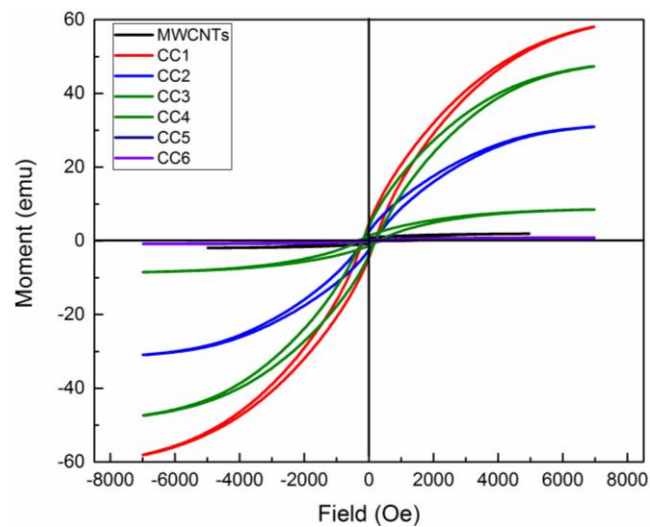


Figure 14 M-H hysteresis curves of MWCNTs and MWCNTs-Co nanocomposite

whereas the M_s value of the nanocomposite is lower than the bulk cobalt value of 161 emu/g [26, 27].

The nanocomposites exhibit characteristics typical of soft magnetic materials, with narrower hysteresis areas and low H_c (coercivity). The nanocomposite's lower M_s compared to MWCNTs suggests that it will require less energy to be demagnetized and will be more responsive to external magnetic fields. However, it is essential to consider that the H_c and M_s are influenced by the size, composition, and form of the nanoparticles. Additionally, the presence of a surfactant layer and surface oxidation can also impact the magnetic properties.

The tiny size of Co nanoparticles results in an increased surface-to-volume ratio, leading to enhanced surface oxidation of the metal nanoparticles and significant spin disorder on the surface. Coercivity's relationship with particle size shows that high H_c values are typically found for single-domain, tiny particles that are not superparamagnetic.

The addition of Fe_3O_4 , $MnFe_2O_4$, and Co nanoparticles to MWCNTs results in an increase in M_s values across all the nanocomposites. This transition from diamagnetic to superparamagnetic and ferromagnetic behavior could contribute to enhanced magnetic loss, leading to increased absorption of the magnetic field associated with microwaves.

4.6 Microwave Absorption

According to transmission line theory, the electromagnetic wave absorption performances of all the composites can be described by the reflection loss (RL) coefficients. Generally, RL ≥ 10 dB is required to meet the demand for practical applications, which means more than 90% absorption of electro-magnetic waves. As demonstrated in Figure 5a, a minimum RL (RL min) value below -30 dB can be achieved by all the samples in the 1-20 GHz range, revealing high-attenuation broadband microwave absorption with a maximum wave absorbing efficiency of >99.9%. It is notable that the MWCNTs/ Fe_3O_4 demonstrates an extremely high electromagnetic wave absorption with a RL min value of -35.22 dB at 14.2 GHz and RL min of -16.74 dB at 19.17 GHz (Figure 5a), which makes it the most competitive absorber among all the composites. Meanwhile, MWCNTs/ $MnFe_2O_4$ and MWCNTs/Co also deliver an excellent absorbing performance of RL min of -31.54 dB (6.57 GHz) and -29.06 dB (6.54 GHz). The effective absorption bandwidth (EAB, frequency region where RL ≤ -3 dB) values of all the samples are close in the region of 13 - 15 GHz and 18-20 GHz for MWCNTs/ Fe_3O_4 , 5-6 GHz for MWCNTs/ $MnFe_2O_4$ and 5-6 GHz for MWCNTs/Co.

The quaternary nanocomposite MWCNTs/ Fe₃O₄/ MnFe₂O₄/ Co exhibits a minimum reflection loss at two different frequencies corresponding to each of the constitute nanocomposite. The RL min value is -32 dB at 8 GHz and -30.47 dB at 16 GHz. The EAB at both RL min is 5 ó10 GHz and 15-18 GHz respectively. The first broadband absorption involve absorption from MnFe₂O₄ and Co nanoparticles whereas the second broadband is due to Fe₃O₄ nanoparticles in the quaternary nanocomposite. The quaternary nanocomposite absorber behaves as a band pass filter, allowing a specific range to pass and absorbing every other frequency. This type of absorber is very useful for stealth application because the microwave from radar detection system needs

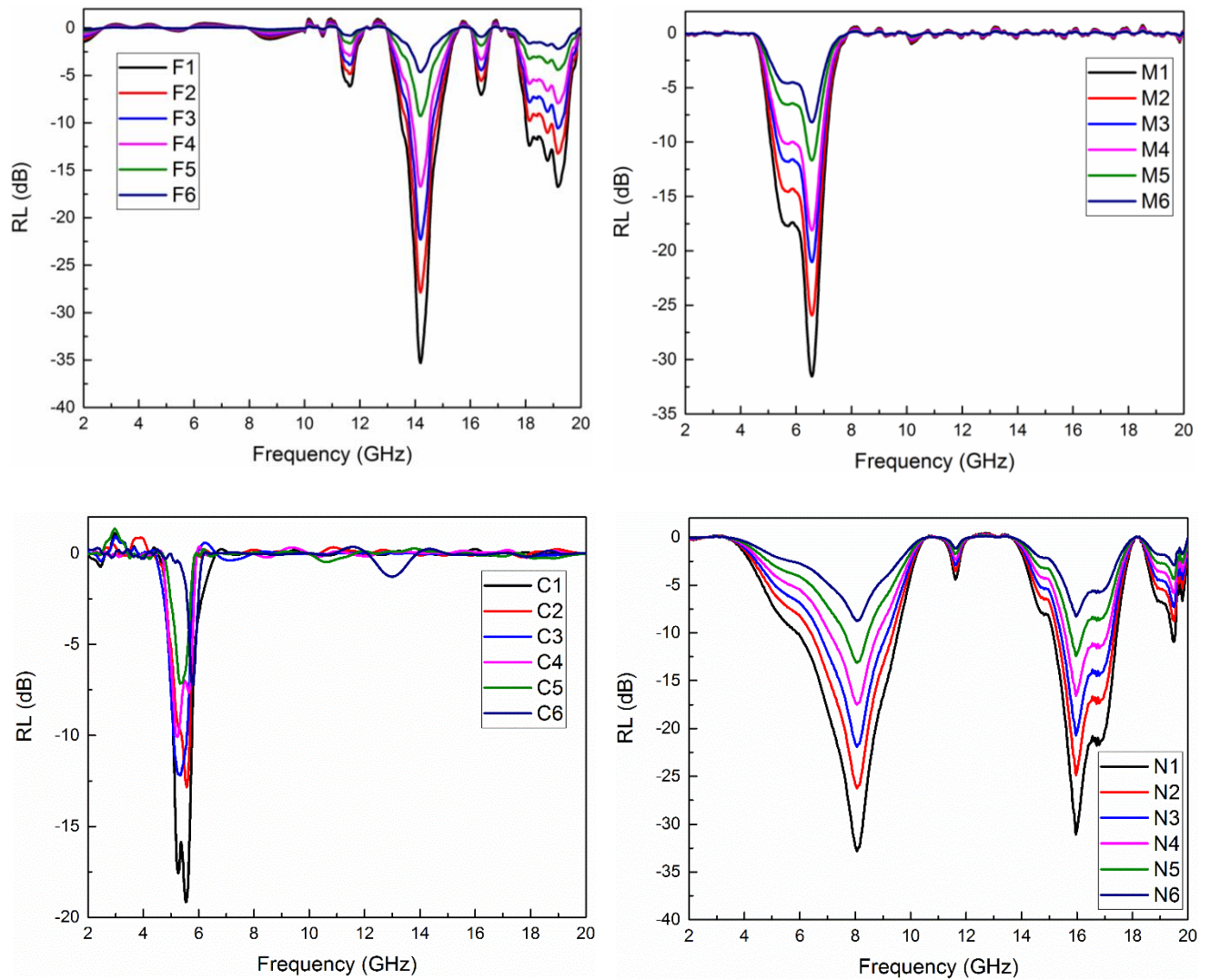


Figure 15 Minimum reflection losses characteristics of MWCNTs/Fe₃O₄, MWCNTs/MnFe₂O₄, MWCNTs/Co, and MWCNTs/MnFe₂O₄/Fe₃O₄/Co quaternary nanocomposite

sto be absorbed by the aircraft, while keeping an open communication link with their own center. This work ensures this band pass absorber by carefully engineering nanoparticles on the surface of MWCNTs.

The nanocomposites containing Fe, Co, and Mn atoms display characteristics of spin magnetization. The Fe_3O_4 and MnFe_2O_4 nanoparticles exhibit an interesting antiferromagnetic coupling phenomenon involving Fe atoms, which contributes to a reduction in saturation magnetization. Under the influence of altering electromagnetic fields, the magnetic moments of Fe, Co, and Mn atoms can undergo resonance, resulting in a favorable magnetic loss capability for absorbing electromagnetic wave energy. Additionally, the dense magnetic field lines originating from the MWCNTs/ Fe_3O_4 / MnFe_2O_4 /Co nanocomposite envelop magnetic materials with appropriate saturation magnetization exhibit magnetic coupling interactions that enhance their magnetic loss capacities. In the context of the MWCNTs nanocomposite, neighboring magnetic particles. The magnetic coupling effect among these Fe_3O_4 , MnFe_2O_4 , and Co nanoparticles leads to the creation of isolated magnetic loss units that form a compact magnetic absorption network. This network effectively amplifies the attenuation of electromagnetic energy. To sum up, the electromagnetic wave absorption mechanism of the synthesized ferromagnetic MWCNTs/ Fe_3O_4 / MnFe_2O_4 /Co nanocomposite primarily involves the conversion of electromagnetic energy into thermal energy through the synergistic interplay of dielectric and magnetic losses. The Fe_3O_4 , MnFe_2O_4 , and Co nanoparticles, along with the hetero-interfaces of MWCNTs, contribute to exceptional electronic dipole polarizations and interfacial polarization relaxations. Concurrently, the conductive MWCNTs network facilitates robust conductive loss through electron migration. Moreover, the ferromagnetic Fe_3O_4 , MnFe_2O_4 , and Co nanoparticles serve as magnetic loss units within the electromagnetic energy absorber system. The notable magnetic coupling interactions among adjacent nanoparticles form a densely interconnected magnetic absorption network. This network, coupled with the magnetic resonance of ferromagnetic atoms, effectively induces magnetic relaxation, thereby dissipating electromagnetic wave energy.

Conclusion

In conclusion, the combination of MWCNTs with Fe_3O_4 , MnFe_2O_4 , and Cobalt nanoparticles has shown promising potential as radar absorbing materials. The nanocomposites exhibit enhanced magnetic properties, with increased M_s values achieved through the attachment of these magnetic nanoparticles. The increase of M_s from 1.9 emu/ g of MWCNTs to 35 emu/ g for MWCNTs- Fe_3O_4 , 20 emu/ g for MWCNTs- MnFe_2O_4 , 60 emu/ g for MWCNTs-Co. Also, the transition from diamagnetic to superparamagnetic and ferromagnetic behavior in the nanocomposites contributes to improved magnetic loss, resulting in higher absorption of the magnetic field associated with microwaves.

The unique properties of these nanocomposites, such as their narrow hysteresis areas and low coercivity, indicate that they possess characteristics of soft magnetic materials, making them suitable for radar absorbing applications. The lower H_c compared to MWCNTs suggests that the nanocomposites will require less energy for demagnetization and will be more sensitive to external magnetic fields, making them effective in attenuating radar signals.

Furthermore, the control of particle size, composition, and form of the nanoparticles plays a crucial role in determining the magnetic properties of the nanocomposites. Additionally, factors like surface oxidation can influence the magnetic characteristics, and surface spin disorder resulting from small nanoparticles further contributes to the overall performance of these materials.

Overall, MWCNTs combined with Fe_3O_4 , MnFe_2O_4 , and Cobalt nanoparticles show great promise as radar absorbing materials due to their enhanced magnetic behavior and increased absorption of microwaves. Continued research and optimization of these nanocomposites hold the potential to advance radar absorbing technologies and contribute to various applications in the fields of defense, communication, and electromagnetic interference shielding.

References

- [1] E. F. Knott, J. F. Shaeffer, and M. T. Tuley, "Radar cross section," 2nd ed ed: Artech House, (1993), p. 611.
- [2] C. A. Balanis, "Advanced engineering electromagnetics," 2nd ed ed: John Wiley & Sons, (2012), p. 1018.
- [3] G. MacFarlane, "Radar camouflage research and development by the Germans," *unpublished notes*, (1945).
- [4] O. HALPERN and J. M. H, "Absorbent For Electromagnetic Waves," ed: OTTO HALPERN, (1960).
- [5] W. LUDWIG, "Resonance Absorber For Electromagnetic Waves," ed: WESCH LUDWIG OP - US 8682461 A 19610202, (1970).
- [6] A. P. Mouritz, "Introduction to aerospace materials," ed: American Institute of Aeronautics and Astronautics ; Woodhead Pub, (2012), p. 621.
- [7] F. Qin and C. Brosseau, "A review and analysis of microwave absorption in polymer composites filled with carbonaceous particles," vol. 111, ed: American Institute of PhysicsAIP, (2012), p. 061301.
- [8] D. Micheli, C. Apollo, R. Pastore, and M. Marchetti, "X-Band microwave characterization of carbon-based nanocomposite material, absorption capability comparison and RAS design simulation," vol. 70, ed: Elsevier, (2010), pp. 400-409.
- [9] L. d. C. Folgueras, E. L. Nohara, R. Faez, and M. C. Rezende, "Dielectric microwave absorbing material processed by impregnation of carbon fiber fabric with polyaniline," *Materials Research*, vol. 10, pp. 95-99, (2007).
- [10] Z. Wang and G.-L. Zhao, "Microwave Absorption Properties of Carbon Nanotubes-Epoxy Composites in a Frequency Range of 2 - 20 GHz," vol. 03, ed: Scientific Research Publishing, Inc., (2013), pp. 17-23.
- [11] C O " M q n c p q y u m c . " F 0 " L c p c u . " C 0 " R 0 " J g t o c p . " Boncel, "From blackness to invisibility (Carbon nanotubes role in the attenuation of and shielding from radio waves for stealth technology," *Carbon*, vol. 126, pp. 31-52, (2018).

- [12] X. Shi, W. You, Y. Zhao, X. Li, Z. Shao, and R. Che, "Multi-scale magnetic coupling of Fe@ SiO₂@ C@Ni yolk@ triple-shell microspheres for broadband microwave absorption," *Nanoscale*, vol. 11, no. 37, pp. 17270-17276, (2019).
- [13] X. Li *et al.*, "One-pot synthesis of CoFe₂O₄/graphene oxide hybrids and their conversion into FeCo/graphene hybrids for lightweight and highly efficient microwave absorber," *Journal of Materials Chemistry A*, vol. 3, no. 10, pp. 5535-5546, (2015).
- [14] K. Ren *et al.*, "Realizing significant dielectric dispersion of composites based on highly conducting silver-coated glass microspheres for wide-band non-magnetic microwave absorbers," *Journal of Materials Chemistry C*, vol. 7, no. 3, pp. 528-542, (2019).
- [15] J. d. C. Dias, I. M. Martin, and M. C. Rezende, "Reflectivity of hybrid microwave absorbers based on NiZn ferrite and carbon black," *Journal of Aerospace Technology and Management*, vol. 4, pp. 267-274, (2012).
- [16] P. Saini, M. Arora, G. Gupta, B. K. Gupta, V. N. Singh, and V. Choudhary, "High permittivity polyaniline barium titanate nanocomposites with excellent electromagnetic interference shielding response," vol. 5, ed: The Royal Society of Chemistry, (2013), pp. 4330-4336.
- [17] M.-G. Han, W. Guo, Y.-H. Wu, M. Liu, and M. L. Hadimani, "Electromagnetic wave absorbing properties and hyperfine interactions of Fe@Cu@Nb@Si@B nanocomposites," *Chinese Physics B*, vol. 23, no. 8, p. 083301, (2014).
- [18] A. Munir, "Microwave Radar Absorbing Properties of Multiwalled Carbon Nanotubes Polymer Composites: A Review," vol. 36, ed: John Wiley & Sons, Ltd, (2017), pp. 362-370.
- [19] B. D. Che, L.-T. T. Nguyen, B. Q. Nguyen, H. T. Nguyen, T. V. Le, and N. H. Nguyen, "Effects of carbon nanotube dispersion methods on the radar absorbing properties of MWCNT/epoxy nanocomposites," *Macromolecular Research*, vol. 22, pp. 1221-1228, (2014).
- [20] A. Joshi, A. Bajaj, R. Singh, P. S. Alegaonkar, K. Balasubramanian, and S. Datar, "Graphene nanoribbon/PVA composite as EMI shielding material in the X band," *Nanotechnology*, vol. 24, no. 45, p. 455705, (2013).

- [21] H. Xing, Y. Liu, Z. Liu, H. Wang, and H. Jia, "Structure and Microwave Absorption Properties of Polyaniline / Zn Ferrite Composites," vol. 13, ed. (2018), pp. 1-12.
- [22] A. Ghasemi, G. R. Gordani, and E. Ghasemi, "Journal of Magnetism and Magnetic Materials Co 2 W hexaferrite nanoparticles-carbon nanotube microwave absorbing nanocomposite," vol. 469, ed: Elsevier B.V., (2019), pp. 391-397.
- [23] J. H. Park, J. Choi, K. Lee, J. Park, J. K. Song, and E. Jeon, "Enhanced Microwave Absorption of CNT Composites Mixing with Fe₃O₄ and Carbonyl Iron," *Archives of Metallurgy and Materials*, vol. 63, (2018).
- [24] Z. Wang, J. Luo, G. L. Zhao, Z. Wang, J. Luo, and G. Lin, "Dielectric and microwave attenuation properties of graphene nanoplatelet epoxy composites Dielectric and microwave attenuation properties of graphene nanoplatelet epoxy composites," vol. 017139, ed, (2015).
- [25] K. Pubby, K. V. Babu, and S. B. Narang, "Magnetic, elastic, dielectric, microwave absorption and optical characterization of cobalt-substituted nickel spinel ferrites," *Materials Science and Engineering: B*, vol. 255, p. 114513, (2020).
- [26] A. R. Bueno, M. L. Gregori, and M. C. Nobrega, "Microwave-absorbing properties of Ni_{0.50}Zn_{0.50} ferrite / carbon nanotube composite in X-band frequencies," *Journal of Magnetism and Magnetic Materials*, vol. 320, no. 6, pp. 864-870, (2008).
- [27] T. Zhao *et al.*, "Synthesis of sandwich microstructured expanded graphite/barium ferrite connected with carbon nanotube composite and its electromagnetic wave absorbing properties," *Journal of Alloys and Compounds*, vol. 712, pp. 59-68, (2017).
- [28] L. Zhong, R. Yu, and X. Hong, "Review of carbon-based electromagnetic shielding materials: film, composite, foam, textile," *Textile Research Journal*, vol. 91, no. 9-10, pp. 1167-1183, (2021).

- [29] X. Chen, H. Liu, D. Hu, H. Liu, and W. Ma, "Recent advances in carbon nanotubes-based microwave absorbing composites," *Ceramics International*, vol. 47, no. 17, pp. 23749-23761, (2021).
- [30] B. Shin, S. Mondal, M. Lee, S. Kim, Y.-I. Huh, and C. Nah, "Flexible thermoplastic polyurethane-carbon nanotube composites for electromagnetic interference shielding and thermal management," *Chemical Engineering Journal*, vol. 418, p. 129282, (2021).
- [31] A. Houbi, Z. A. Aldashevich, Y. Atassi, Z. B. Telmanovna, M. Saule, and K. Kubanych, "Microwave absorbing properties of ferrites and their composites: A review," *Journal of Magnetism and Magnetic Materials*, vol. 529, p. 167839, (2021).
- [32] Y. Zhou, L. Chen, M. Jian, and Y. Liu, "Recent research progress of ferrite multielement microwave absorbing composites," *Advanced Engineering Materials*, vol. 24, no. 12, p. 2200526, (2022).
- [33] I. S. Seo and W. S. Chin, "Characterization of electromagnetic properties of polymeric composite materials with free space method," *Composite Structures*, vol. 66, no. 1-4, pp. 533-542, (2004).
- [34] N. E. Prasad and R. J. Wanhill, *Aerospace materials and material technologies*. Springer, (2017).
- [35] W.-T. W. Group, "IEEE Std 521-2002 (Revision of IEEE Std 521-1984)-IEEE Standard Letter Designations for Radar-Frequency Bands," *AES-IEEE Aerospace and Electronic Systems Society*, (2009).
- [36] E. F. Knott, J. F. Schaeffer, and M. T. Tulley, *Radar cross section*. SciTech Publishing, (2004).
- [37] V. Petrov and V. Gagulin, "Microwave absorbing materials," *Inorganic Materials*, vol. 37, pp. 93-98, (2001).
- [38] B. Zohuri, *Radar energy warfare and the challenges of stealth technology*. Springer, (2020).
- [39] L. Huang *et al.*, "Challenges and future perspectives on microwave absorption based on two-dimensional materials and structures," *Nanotechnology*, vol. 31, no. 16, p. 162001, (2020).

- [40] F. Wang *et al.*, "Microwave absorption properties of 3D cross-linked Fe/C porous nanofibers prepared by electrospinning," *Carbon*, vol. 134, pp. 264-273, (2018).
- [41] L. Wang *et al.*, "Synthesis and microwave absorption property of flexible magnetic film based on graphene oxide/carbon nanotubes and Fe₃O₄ nanoparticles," *Journal of Materials Chemistry A*, vol. 2, no. 36, pp. 14940-14946, (2014).
- [42] T. Indrusiak, I. M. Pereira, A. P. Heitmann, J. G. Silva, Â. M. Denadai, and B. G. Soares, "Epoxy/ferrite nanocomposites as microwave absorber materials: effect of multilayered structure," *Journal of Materials Science: Materials in Electronics*, vol. 31, pp. 13118-13130, (2020).
- [43] W. Jang, S. Mallesh, S. B. Lee, and K. H. Kim, "Microwave absorption properties of core-shell structured FeCoNi@ PMMA filled in composites," *Current Applied Physics*, vol. 20, no. 4, pp. 525-530, (2020).
- [44] P.-J. Liu, Z.-J. Yao, V. M. H. Ng, J.-T. Zhou, Z.-H. Yang, and L.-B. Kong, "Enhanced microwave absorption properties of double-layer absorbers based on spherical NiO and Co_{0.2}Ni_{0.4}Zn_{0.4}Fe₂O₄ ferrite composites," *Acta Metallurgica Sinica (English Letters)*, vol. 31, pp. 171-179, (2018).
- [45] Y. Liu, X. Liu, and X. Wang, "Synthesis and microwave absorption properties of Ni_{0.5}Zn_{0.5}Mn spinel ferrites," *Advances in Applied Ceramics*, vol. 114, no. 2, pp. 82-86, 2015.
- [46] D. Jenn, *Radar and laser cross section engineering*. American Institute of Aeronautics and Astronautics, Inc., (2005).
- [47] P. Rajyalakshmi and G. Raju, "Characteristics of radar cross section with different objects," *International Journal of Electronics and Communication Engineering*, vol. 4, no. 2, pp. 205-216, (2011).
- [48] C. K. Yuzcelik, "Radar absorbing material design," Monterey, California. Naval Postgraduate School, (2003).
- [49] I. Nicolaescu, "Radar absorbing materials used for target camouflage," *Journal of optoelectronics and advanced materials*, vol. 8, no. 1, p. 333, (2006).

- [50] K. Vinoy and R. Jha, "Trends in radar absorbing materials technology," *Sadhana*, vol. 20, pp. 815-850, (1995).
- [51] S. Kim, S. Jo, K. Gueon, K. Choi, J. Kim, and K. Churn, "Complex permeability and permittivity and microwave absorption of ferrite-rubber composite at X-band frequencies," *IEEE Transactions on Magnetics*, vol. 27, no. 6, pp. 5462-5464, (1991).
- [52] P. Xie *et al.*, "Tunneling-induced negative permittivity in Ni/MnO nanocomposites by a bio-gel derived strategy," *Journal of Materials Chemistry C*, vol. 8, no. 9, pp. 3029-3039, (2020).
- [53] X. Sun *et al.*, "Laminated magnetic graphene with enhanced electromagnetic wave absorption properties," *Journal of Materials Chemistry C*, vol. 1, no. 4, pp. 765-777, (2013).
- [54] C. Jayalakshmi, A. Inamdar, A. Anand, and B. Kandasubramanian, "Polymer matrix composites as broadband radar absorbing structures for stealth aircrafts," *Journal of Applied Polymer Science*, vol. 136, no. 14, p. 47241, (2019).
- [55] E. Michielssen, J.-M. Sajer, S. Ranjithan, and R. Mittra, "Design of lightweight, broad-band microwave absorbers using genetic algorithms," *IEEE Transactions on Microwave Theory and Techniques*, vol. 41, no. 6, pp. 1024-1031, (1993).
- [56] A. Teber, "Development of radar absorbing materials (RAMs) based on nano-structured magnetic materials and applications," (2017).
- [57] A. Nicolson and G. Ross, "Measurement of the intrinsic properties of materials by time-domain techniques," *IEEE Transactions on instrumentation and measurement*, vol. 19, no. 4, pp. 377-382, (1970).
- [58] G. Wu, Y. He, H. Zhan, Q. Q. Shi, and J. N. Wang, "A novel Fe₃O₄/carbon nanotube composite film with a cratered surface structure for effective microwave absorption," *Journal of Materials Science: Materials in Electronics*, vol. 31, pp. 11508-11519, 2020.
- [59] P. Saville, "Review of Radar Absorbing Materials," vol. 23, ed, (2005), p. 62.
- [60] P. Dixon, "Theory and application of RF/microwave absorbers," *Techn. Ber. Emerson & Cuming Microwave Products*, (2012).

- [61] A. Hasnain *et al.*, "Development of an economic and effective microwave absorber," in *2007 Asia-Pacific Conference on Applied Electromagnetics, 2007*: IEEE, pp. 1-5.
- [62] C. L. Holloway, R. R. Delyser, R. F. German, P. McKenna, and M. Kanda, "Comparison of electromagnetic absorber used in anechoic and semi-anechoic chambers for emissions and immunity testing of digital devices," *IEEE Transactions on Electromagnetic Compatibility*, vol. 39, no. 1, pp. 33-47, (1997).
- [63] W. Emerson, "Electromagnetic wave absorbers and anechoic chambers through the years," *IEEE Transactions on Antennas and Propagation*, vol. 21, no. 4, pp. 484-490, (1973).
- [64] X. C. Tong, *Advanced materials and design for electromagnetic interference shielding*. CRC press, (2016).
- [65] L. K. Neher, "Nonreflecting background for testing microwave equipment," ed: Google Patents, (1953).
- [66] W. Dallenbach and W. Kleinstueber, "Reflection and absorption of decimeter-waves by plane dielectric layers," *Hochfreq. u Elektroak*, vol. 51, pp. 152-156, (1938).
- [67] F. Mayer, "High frequency broadband absorption structures," ed: Google Patents, (1999).
- [68] K. Hatakeyama and T. Inui, "Electromagnetic wave absorber using ferrite absorbing material dispersed with short metal fibers," *IEEE Transactions on Magnetics*, vol. 20, no. 5, pp. 1261-1263, (1984).
- [69] T. M. Connolly and E. J. Luoma, "Microwave absorbers," ed: Google Patents, (1977).
- [70] P. Liu, S. Gao, Y. Wang, Y. Huang, Y. Wang, and J. Luo, "Core-shell CoNi@graphitic carbon decorated on B, N-codoped hollow carbon polyhedrons toward lightweight and high-efficiency microwave attenuation," *ACS Applied Materials & Interfaces*, vol. 11, no. 28, pp. 25624-25635, (2019).

- [71] M. S. Cao *et al.*, "Electromagnetic response and energy conversion for functions and devices in low dimensional materials," *Advanced Functional Materials*, vol. 29, no. 25, p. 1807398, (2019).
- [72] Z. Wu, K. Pei, L. Xing, X. Yu, W. You, and R. Che, "Enhanced microwave absorption performance from magnetic coupling of magnetic nanoparticles suspended within hierarchically tubular composite," *Advanced Functional Materials*, vol. 29, no. 28, p. 1901448, (2019).
- [73] B. Quan *et al.*, "Defect engineering in two common types of dielectric materials for electromagnetic absorption applications," *Advanced Functional Materials*, vol. 29, no. 28, p. 1901236, (2019).
- [74] W.-L. Song, M.-S. Cao, Z.-L. Hou, X.-Y. Fang, X.-L. Shi, and J. Yuan, "High dielectric loss and its monotonic dependence of conducting-dominated multiwalled carbon nanotubes/silica nanocomposite on temperature ranging from 373 to 873 K in X-band," *Applied physics letters*, vol. 94, no. 23, (2009).
- [75] L. Liang *et al.*, "Multifunctional magnetic Ti₃C₂T_x MXene/graphene aerogel with superior electromagnetic wave absorption performance," *ACS nano*, vol. 15, no. 4, pp. 6622-6632, (2021).
- [76] W. Wei *et al.*, "Light-weight gadolinium hydroxide@ polypyrrole rare-earth nanocomposites with tunable and broadband electromagnetic wave absorption," *ACS applied materials & interfaces*, vol. 11, no. 13, pp. 12752-12760, (2019).
- [77] W. You, W. She, Z. Liu, H. Bi, and R. Che, "High-temperature annealing of an iron microplate with excellent microwave absorption performance and its direct micromagnetic analysis by electron holography and Lorentz microscopy," *Journal of Materials Chemistry C*, vol. 5, no. 24, pp. 6047-6053, (2017).
- [78] X. J. Zhang *et al.*, "Tunable high performance microwave absorption of Co₁₋₆ xS hollow spheres constructed by nanosheets within ultralow filler loading," *Advanced Functional Materials*, vol. 28, no. 49, p. 1800761, (2018).
- [79] T. Zhu, S. Chang, Y.-F. Song, M. Lahoubi, and W. Wang, "PVP-encapsulated CoFe₂O₄/rGO composites with controllable electromagnetic wave absorption performance," *Chemical Engineering Journal*, vol. 373, pp. 755-766, (2019).

- [80] S. Gao, S.-H. Yang, H.-Y. Wang, G.-S. Wang, and P.-G. Yin, "Excellent electromagnetic wave absorbing properties of two-dimensional carbon-based nanocomposite supported by transition metal carbides Fe₃C," *Carbon*, vol. 162, pp. 438-444, (2020).
- [81] S. Biswas, I. Arief, S. S. Panja, and S. Bose, "Absorption-dominated electromagnetic wave suppressor derived from ferrite-doped cross-linked graphene framework and conducting carbon," *ACS applied materials & interfaces*, vol. 9, no. 3, pp. 3030-3039, (2017).
- [82] K. Zhang, X. Gao, Q. Zhang, T. Li, H. Chen, and X. Chen, "Preparation and microwave absorption properties of asphalt carbon coated reduced graphene oxide/magnetic CoFe₂O₄ hollow particles modified multi-wall carbon nanotube composites," *Journal of Alloys and Compounds*, vol. 723, pp. 912-921, (2017).
- [83] G. Tong, F. Liu, W. Wu, F. Du, and J. Guan, "Rambutan-like Ni/MWCNT heterostructures: easy synthesis, formation mechanism, and controlled static magnetic and microwave electromagnetic characteristics," *Journal of Materials Chemistry A*, vol. 2, no. 20, pp. 7373-7382, (2014).
- [84] H. Lv, X. Liang, G. Ji, H. Zhang, and Y. Du, "Porous three-dimensional flower-like Co/CoO and its excellent electromagnetic absorption properties," *ACS applied materials & interfaces*, vol. 7, no. 18, pp. 9776-9783, (2015).
- [85] V. Shukla, "Review of electromagnetic interference shielding materials fabricated by iron ingredients," *Nanoscale Advances*, vol. 1, no. 5, pp. 1640-1671, (2019).
- [86] L. Wang *et al.*, "Confined magnetic dielectric balance boosted electromagnetic wave absorption," *Small*, vol. 17, no. 30, p. 2100970, (2021).
- [87] L. Wang *et al.*, "Oriented polarization tuning broadband absorption from flexible hierarchical ZnO arrays vertically supported on carbon cloth," *Small*, vol. 15, no. 18, p. 1900900, (2019).
- [88] W. Liu *et al.*, "Metal organic-frameworks derived porous carbon-wrapped Ni composites with optimized impedance matching as excellent lightweight electromagnetic wave absorber," *Chemical Engineering Journal*, vol. 313, pp. 734-744, (2017).

- [89] Z.-J. Li *et al.*, "Unusual continuous dual absorption peaks in Ca-doped BiFeO₃ nanostructures for broadened microwave absorption," *Nanoscale*, vol. 8, no. 19, pp. 10415-10424, (2016).
- [90] L. Liu, W. Ma, and Z. Zhang, "Macroscopic carbon nanotube assemblies: preparation, properties, and potential applications," *Small*, vol. 7, no. 11, pp. 1504-1520, (2011).
- [91] X. Qi *et al.*, "Metal-free carbon nanotubes: synthesis, and enhanced intrinsic microwave absorption properties," *Scientific reports*, vol. 6, no. 1, p. 28310, (2016).
- [92] A. Katsounaros, K. Z. Rajab, Y. Hao, M. Mann, and W. I. Milne, "Microwave characterization of vertically aligned multiwalled carbon nanotube arrays," *Applied Physics Letters*, vol. 98, no. 20, (2011).
- [93] Z. Yang *et al.*, "Broadband polarization-insensitive microwave-absorbing composite material based on carbon nanotube film metamaterial and ferrite," *Journal of Applied Physics*, vol. 125, no. 18, (2019).
- [94] J. Hu, T. Zhao, X. Peng, W. Yang, X. Ji, and T. Li, "Growth of coiled amorphous carbon nanotube array forest and its electromagnetic wave absorbing properties," *Composites Part B: Engineering*, vol. 134, pp. 91-97, (2018).
- [95] H. Sun *et al.*, "Cross-Stacking Aligned Carbon-Nanotube Films to Tune Microwave Absorption Frequencies and Increase Absorption Intensities," *Advanced Materials*, vol. 26, no. 48, pp. 8120-8125, (2014).
- [96] M. Naidu, K. Ramji, B. Santhosi, T. Shami, H. B. Baskey, and B. Satyanarayana, "Enhanced microwave absorption of quartic layered epoxy-mwcnt composite for radar applications," *Advanced Composites Letters*, vol. 26, no. 4, p. 096369351702600405, (2017).
- [97] Z. Liu *et al.*, "Broadening microwave absorption via a multi-domain structure," *APL Materials*, vol. 5, no. 4, (2017).
- [98] C. Tian *et al.*, "Constructing uniform core-shell PPy@ PANI composites with tunable shell thickness toward enhancement in microwave absorption," *ACS applied materials & interfaces*, vol. 7, no. 36, pp. 20090-20099, (2015).

- [99] M. Huang *et al.*, "Multidimension controllable synthesis of MOF derived Co@ N doped carbon composite with magnetic dielectric synergy toward strong microwave absorption," *Small*, vol. 16, no. 14, p. 2000158, (2020).